Probing Entanglement with Holography

Heli Takko

Master's thesis
UNIVERSITY OF HELSINKI
Department of Physics

Helsinki, May 3, 2021

HELSINGIN YLIOPISTO — HELSINGFORS UNIVERSITET — UNIVERSITY OF HELSINKI

Tiedekunta — Fakultet — Faculty	Laitos — Institution — Department
Faculty of Science	Department of Physics

Tekijä — Författare — Author
Heli Takko

Työn nimi — Arbetets titel — Title

Probing Entanglement with Holography

Oppiaine — Läroämne — Subject
Master's programme in Theoretical and Computational methods

Työn laji — Arbetets art — Level	Aika — Datum — Month and year	Sivumäärä — Sidoantal — Number of pages
Master's thesis	May 3, 2021	48

Tiivistelmä — Referat — Abstract

Quantum entanglement is one of the biggest mysteries in physics. In gauge field theories, the amount of entanglement can be measured with certain quantities. For an entangled system, there are correlations with these measured quantities in both time and spatial coordinates that do not fit into the understanding we currently hold about the locality of the measures and correlations. Difficulties in obtaining probes for entanglement in gauge theories arise from the problem of nonlocality. It can be stated as the problem of decomposing the space of the physical states into different regions.

In this thesis, we focus on a particular supersymmetric Yang-Mills theory that is holographically dual to a classical gravity theory in an asymptotically anti de Sitter spacetime. We introduce the most important holographic probes of entanglement and discuss the inequalities obtained from the dual formulation of the entanglement entropy. We introduce the subregion duality as an interesting conjecture of holography that remains under research. The understanding of the subregion duality is not necessarily solid in arbitrary geometries, as new results that suggest either a violation of the subregion duality or act against our common knowledge of the holography by reconstructing the bulk metric beyond the entanglement wedge.

This thesis will investigate this aspect of subregion duality by evaluating the bulk probes such as Wilson loop for two different geometries (deconfining and confining). We aim to find whether or not these probes remain inside of the entanglement wedge. We find that, for both geometries in four dimensions, the subregion duality is not violated. In other words, the reduced CFT state does not encode information about the bulk beyond the entanglement wedge. However, we can not assume this is the case with arbitrary geometries and therefore, this topic will remain under our interest for future research.

Avainsanat — Nyckelord — Keywords

Säilytyspaikka — Förvaringsställe — Where deposited

Muita tietoja — Övriga uppgifter — Additional information

Contents

1 Motivation and introduction

One of the most interesting topics of the cutting-edge research in areas such as quantum field theory is to describe and explain the quantum entanglement. Quantum mechanics has proven itself on being the fundamental basis of our world, and explaining the entanglement as a phenomenon would be the next big step in the path to better understanding of our universe. Steps towards this goals have been made particularly in the area of the holographic duality [35]. While the quantum field theories alone are incapable of describing and explaining the entanglement of gravitational interaction, the holography provides new, efficient tools. In general, the holographic principle rests on a duality of certain quantum field theories (QFTs) with gravitational theories in higher dimension. In other words, the holographic QFTs with fixed spacetime geometry correspond to a gravitational theory with a boundary described with this same geometry. Thus, the problems and calculations in such holographic QFTs can be calculated and solved using the methods of general relativity. In particular, we concentrate on the AdS/CFT correspondence as an example of the holographic duality. The reason of major interest towards AdS/CFT comes from the fact it gives connection between calculations in perturbative string theory and calculations in certain gauge field theory without perturbations. In other words, these non-perturbative calculations correspond to strong coupling, in which the results are significantly harder to obtain in the frame of field theory [37]. Therefore, we shall take the examined QFT to the limit of a large number of degrees of freedom and large coupling constant. This allows us to relate the QFT with perturbative string theory and access the tools of holographic duality.

This thesis will concentrate on introducing the phenomena of quantum entanglement in terms of holographic duality and discuss the ways and probes we can examine this phenomenon with. In this first chapter, we take an introduction-level look into the basics of the AdS/CFT correspondence and its mathematical formulation. Continuing to the Chapter 2, we shall introduce the probes of the holography. These probes include for example the Wilson loops, two-point functions and entanglement entropy. In addition, we will discuss the subregion duality and the details of entanglement wedge and its cross section. We describe how these probes are obtained using the holographic principle and further, how they help us understand the entanglement as a phenomenon. In the Chapter 3, we discuss the entanglement entropy inequalities. First, we introduce the fundamental inequalities and then move on to the holographic entropy cone and to the recent research results on the entropy inequalities. In addition, we take detailed look of the conjecture of the entanglement wedge reconstruction that would possibly violate the subregion duality. Furthermore, the probes introduced and discussed in the Chapter 2 reveal their main purpose for this thesis in the Chapter 4. We will evaluate the probes for two different bulk geometries and check whether or not they fall inside the entanglement wedge. Finally, in the Chapter 5, we conclude the results and discuss about the conclusions and possibilities for future research about this topic.

Starting with the introduction to the holographic duality, the first and most well-known example of it is the AdS/CFT correspondence that describes the duality

between conformal field theory (CFT) and quantum gravity [2]. An important example of the AdS/CFT correspondence is the family of black hole geometries. At that case we have AdS_{d+1} background which is dual to thermal state of CFT. The holographic duality as we know it today was introduced by Maldacena [36]. However, We can start the discussion from the black hole entropy

$$S_{BH} = \frac{A}{4l_P^2}, \tag{1.1}$$

also known as the Bekenstein-Hawking entropy [45]. We could also state that the holographic principle was introduced from string theory by considering a system of branes and taking it to the limit of low energy [21]. For example, when we take the type IIB string theory with N branes, we can consider the low-energy limit and therefore use the particular conformal field theory known as the maximally supersymmetric Yang-Mills theory, also referred as the SYM theory. We will talk more about the properties and importance of the Yang-Mills theory later on.

In (1.1), A represents the area of an event horizon and l_P is the Planck length. We can think the black hole entropy from the field theory point of view. Consider the degrees of freedom beyond the horizon. If we trace over them, we can obtain the entanglement entropy associated with the horizon. It turns out to be proportional to the area of the given boundary, which is analogous to the form of the Bekenstein-Hawking entropy.

In more detail, on the side of gravity, the boundary of spatial volume encodes all the information about the volume itself. To get an idea how the duality works, the number of degrees of freedom on each side of the correspondence needs to be matched first. Since the degrees of freedom are measured by the entropy, for a spatial region R_{d-1} with d-dimensional spacetime in CFT side we have

$$S_{QFT} \propto Vol(R_{d-1}). \tag{1.2}$$

Then, for spacetime on gravity side with $d+1$ dimensions, the entropy follows (1.1), and a spatial region R_d on the gravity side in $d+1$ dimensions is bounded by a manifold with $d-1$ dimensions. This can be expressed as

$$R_{d-1} = \partial R_d. \tag{1.3}$$

From this, it is straightforward to see that indeed, the entropy on the gravity side is proportional to the area of the boundary ∂R_d. Furthermore, this area is proportional to the volume of the spatial region on the CFT side with $d-1$ dimensions, namely

$$S_{GR}(R_d) \propto Area(\partial R_d) \propto Vol(R_{d-1}). \tag{1.4}$$

In particular, we demand the background geometry to be asymptotically AdS, since it results in conformal boundary geometry in the limit of UV. The relation 1.4 arises from the conformal invarience of the considered QFT, i.e. the field theory is at fixed point of the renormalization group. Renormalization group is tool that helps to investigate the behavior of physical system at varying scales. The renormalization

group flow is then a group of scale transformations, with space determined by the coupling constants. It follows that, this flow allows the original CFT to be equivalent to the one described with the scale transformations [12][39]. The renormalization group is useful with many CFTs, but not in the case of gravity. Therefore, in this thesis we focus on the probes and tools of holography, and to the CFTs that are dual to gravitational theories. However, worth of mentioning is that all CFTs are not necessarily dual. Thus, the question of finding the subset of CFTs with gravitational duals is under active research, one example being a set of dual CFTs proposed in [9].

For anti-de Sitter spacetime, we can write the line element in $d+1$ dimensions as

$$ds^2 = \frac{L^2}{z^2}(-dt^2 + d\vec{x}^2 + dz^2), \tag{1.5}$$

which is better known as the Poincaré patch. It originates from the Poincaré invariance in d dimensions [37]. However, we must note that the Poincaré coordinates do not cover the whole space. The reason it is called a patch to begin with, is that it only covers a certain part of the whole space. This gives a reason to look at the metric with so called global coordinates that do cover all of the space, with $\tau \in [0, 2\pi]$ and $\rho \in \mathbb{R}^+$:

$$ds^2_{\text{global}} = R^2(-\cosh^2\rho d\tau^2 + d\rho^2 + \sinh^2\rho d\vec{\Omega}^2_{d-2}). \tag{1.6}$$

Here $d\vec{\Omega}^2_{d-2}$ marks the $(d-2)$-dimensional 2-sphere metric. We can make a substitution of $\tan\theta = \sinh\rho$, where θ is defined in two dimensions as $-\pi/2 \leq \theta \leq \pi/2$ and for other dimensions as $0 \leq \theta \leq \pi/2$. The metric can be then written as

$$ds^2_{\text{global}} = \frac{R^2}{\cos^2\theta}(-d\tau^2 + d\theta^2 + \sin^2\theta d\vec{\Omega}^2_{d-2}). \tag{1.7}$$

Now, the part of the space that is covered by the Poincaré coordinates is called the Poincaré patch, and it covers a triangle-like area of the whole space. If we mark $\Omega^i = \sin\theta_1\cos\theta_1, \ldots, \sin\theta_1\sin\theta_2, \ldots, \sin\theta_{d-1}$ s.t. the relation $\Omega_i^2 + \cos^2\theta_1 = 1$ is satisfied, then the Poincaré coordinates (1.5) are connected to the global ones by the following relations:

$$z = \frac{L}{\cosh\rho\cos\tau - \sinh\rho\cos\theta_1} \tag{1.8}$$

$$t = z\cosh\rho\sin\tau \tag{1.9}$$

$$x^i = z\Omega^i\sinh\rho. \tag{1.10}$$

The reason to use the Poincaré patch with the holographic calculation is that it is particularly convenient on describing the dual spacetimes. More importantly, it allows us to investigate the field theory living on the Minkowski spacetime instead on a sphere. Namely, we can treat the d-dimensional Poincaré as the conformal group.

In (1.5), the L represents the anti-de Sitter radius and z the coordinate corresponding to the extra dimension. This line element gives AdS a boundary at $z = 0$

which furthermore yields the geometry of AdS that we are particularly interested in. Important note about the boundary geometry is that it is only one of the choices in the group of geometries with same causal structure.

On the other side of the correspondence, we have conformal field theory. Such field theory is both relativistic and invariant under a set of certain spacetime transformations called conformal group, in addition to having angle-preserving transformations. The conformal group is isomorphic to the group $SO(d, 2)$, which makes the connection to AdS_{d+1} clear. The Poincaré group is the symmetry group of relativistic field theory for flat spacetime [42], and the Poincaré transformations

$$x^\mu \to \Lambda^\mu_\nu x^\nu + a^\mu \tag{1.11}$$

are isometries of a flat spacetime. For the transformations in CFTs that preserve angles, a good example is scale transformation:

$$x^\mu \to \lambda x^\mu. \tag{1.12}$$

Even though scale transformations are part of conformal transformations like Poincaré transformations, it is obvious that the scale transformations do not belong to the Poincaré group. In fact, the conformal group can be identified as the set of $\mathbb{R}^d$ Minkowski spacetime which leaves angles, but not necessary lengths, invariant [21]. An important property of CFTs is that one can always find a special set of operators, i.e. local operators that transform simply under conformal transformations. For example, the primary operators transform under dilatation operator as

$$\mathcal{O}'(x') = \lambda^{-\Delta}\mathcal{O}. \tag{1.13}$$

However, when we are considering the states in CFT, we can not tell whether or not they are holographic based on the transformation properties mentioned above. The way of distinguishing the holographic states from the ones that are not is to check whether their mutual information $I(A : B)$, defined with the entanglement proposed by the Ryu-Takayanagi proposal entropy S as

$$I(A : B) = S(A) + S(B) - S(AB), \tag{1.14}$$

follows the so called monogamy inequality

$$I(A : BC) \geq I(A : B) + I(A : C), \tag{1.15}$$

that we will return to later in the Chapter 3 when discussing the inequalities of holography further.

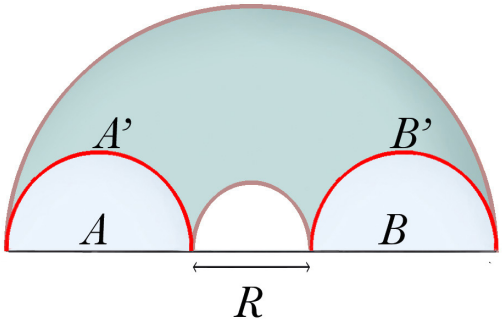

Figure 1: For CFT with two dimensions, the mutual information between two disjoint areas is calculated using the extremal surfaces shown in the figure. The length of the light pink line gives the entanglement entropy of AB, that is $S(AB)$ and correspondingly, the length of the red curves correspond to $S(A)$ and $S(B)$. These entropies are then used to evaluate the mutual information.

2 Probes in holographic duality

We have chosen few of the probes in AdS/CFT to evaluate. The following background introduction of the probes clarifies the reason we chose these probes. We include few words about the Yang-Mills theory, that is a strongly coupled quantum theory raising from the Lie group. As we will see, particularly useful case is the supersymmetric Yang-Mills theory in four dimensions, i.e. $\mathcal{N} = 4$ SYM. This one corresponds to a field theory with 4 supersymmetries relating the boson and fermion fields. Next, we will talk little bit about the algebra and notations associated with the Yang-Mills theory in general.

For a compact Lie group G, for example the $SU(N)$ and $SO(N)$, there is associated Lie algebra with Hermitian generators T^α [37] satisfying

$$[T^\alpha, T^\beta] = if^{\alpha\beta\gamma}T^\gamma, \tag{2.1}$$

where the $f^{\alpha\beta\gamma}$ marks Lie algebra's structure constants. For $SU(N)$ group, the indices go as $\alpha, \beta, \gamma = 1 \ldots N^1 - 1$. These generators need to be further normalized, and typically in the current context we use the following normalization for the generators:

$$\mathrm{Tr}(T^\alpha T^\beta) = \frac{1}{2}\delta^{\alpha\beta}. \tag{2.2}$$

Now, for matter fields with $G = SU(N)$, we can use the gauge field $A_\mu = A_\mu^\alpha T^\alpha$, that is also known as the connection. We introduce the covariant derivative of our state vector ψ carrying the field as

$$\mathcal{D}_\mu\psi = \partial_\mu\psi - ieA_\mu\psi, \tag{2.3}$$

where e is for charge, which in our case we could normalize to one. Moreover, using A_μ, the field strength is defined as within Lie algebra (also known as the curvature), and can be written as

$$F_{\mu\nu} = \partial_\mu A_\nu - \partial_\nu A_\mu - ig[A_\mu, A_\nu]. \tag{2.4}$$

This formulation can be further used to introduce the action of Yang-Mills theory with a coupling constant g [37]:

$$S_{YM} = -\frac{1}{2g^2}\int d^4x \mathrm{Tr} F^{\mu\nu}F_{\mu\nu}. \tag{2.5}$$

The set of all transformations that belong to this symmetry group can be referred as its gauge group. However, we must note that typically, the gauge group refers to $SU(N)$ or $SO(N)$, and the symmetries of Poincaré are considered separately. The gauge symmetry is not to be confused with an actual physical symmetries of the system, but remind ourselves that gauge symmetry takes us from one state to another. Thus, in the description of the system, it is a redundancy. This redundancy is one of the key reasons to use the Yang-Mills theory: The gauge fields with redundancy gives us the possibility to use various properties of the system. Namely, when working with Yang-Mills theory we can for example obtain the degrees of freedom in every generator T^α from the rank of the gauge group. Analogously to the connections mentioned in general relativity, such as Levi-Civita connection, in Yang-Mills theory we can use the connections to describe the parallel transport on a given manifold with appropriate electric charge γ. For the connection A_μ of a particle on a worldline $x^\mu(\tau)$, the parallel transportation is written as

$$i\frac{d\omega}{d\tau} = \frac{dx^\mu}{d\tau}\gamma A_\mu(x)\omega. \tag{2.6}$$

From this, we can then further introduce the probes that are crucial for the discussion and calculations performed later on. The key is that following the presented Yang-Mills theory, we can use the holographic principle in our field theory based calculations to make them easier to evaluate. The calculations via holography are much simpler since it allows us to reduce them to the evaluation of the geodesics and parallel transport. This is significantly simpler than trying to evaluate functions purely in the quantum field theories, that in many cases is an impossible task to perform. In the following chapters, we will discuss further some of these calculations through holography.

2.1 Entanglement entropy

First and very fundamental probe we introduce is the quantum entanglement entropy. Quantum entanglement is a property of a quantum system which means that, it is one of the fundamental factors distinguishing the quantum physics from classical physics. If a quantum state cannot be presented independently from another, the state is described as an entangled state. One way to measure the amount of entanglement in a system is the entanglement entropy. It can be described as the measure of the uncertainty in a quantum system. Entropy itself is not restricted to quantum systems only, but in theory of quantum information, we use formalism different from the classical formulation of the entropy in information theory.

The classical formulation of the entropy in the information theory is called the *Shannon entropy*. For discrete random variable X with realizations at $X = x$, the

probability distribution $P(x)$ with $0 \leq P(x) \leq 1$ has the Shannon entropy $H(X)$ as follows:

$$H(X) = -\sum_{x \in X} P(x)\mathrm{lg}(P(x)) = \langle -\log_2(P(x))\rangle. \tag{2.7}$$

If we denote the number of possible values for X with n, then the Shannon entropy reaches its maximum value at $H(X) = \mathrm{lg}(n)$, which corresponds to the probability distribution at $P(x) = 1/n$. For two random variables X_1 and X_2, we have the Shannon entropy simply as

$$H(X_1, X_2) = -\sum_{x_1 \in X_1, x_2 \in X_2} P(x_1, x_2)\mathrm{lg}(P(x_1, x_2)). \tag{2.8}$$

We can then focus on the quantum equivalent of the information and therefore continue in the frame of quantum mechanics. When talking about entangled quantum states, it is important to introduce the density operator that represents the state. Through the density operator ρ, the state can be described either as a pure state or a mixed state [41]. For the pure states, the density operator satisfies $\rho^2 = \rho$. This means that, the pure state can be constructed and described purely by the Hilbert space state vectors. For mixed states, this is not the case. Instead, the density operator plays more crucial role with mixed states, for which we have $\rho^2 \neq \rho$. In general, ρ is Hermitian and thus satisfies the self-adjointness $\rho^\dagger = \rho$. In addition, it has a unit trace, $\mathrm{Tr}(\rho) = 1$ and satisfies non-negativity. Furthermore, the density operator can be presented in terms of its eigenvectors $\{|i\rangle\}$ and their eigenvalues (which here can be understood as the probability of state being $\{|i\rangle\}$) p_i as

$$\rho = \sum_i p_i |i\rangle\langle i|. \tag{2.9}$$

Let us now consider two subsystems A and B forming a bipartite system in a pure state. We mark the orthonormal basis vectors of these subsystems as $\{|j\rangle_A\}$ and $\{|k\rangle_B\}$. These bases are part of the Hilbert spaces $\mathcal{H}_A$ and $\mathcal{H}_B$. Now, a composite system of these in case of a pure state is described with the pure state density matrix

$$\rho = |\psi\rangle\langle\psi| \tag{2.10}$$

$$= \sum_{j,k} a_{jk}|j_A\rangle \otimes |k_B\rangle \sum_{j,k} \langle j_A| \otimes \langle k_B|, \tag{2.11}$$

where the sum of coefficients is normalized to one. Now, if we define states $|\psi_i^A\rangle$ and $|\psi_i^B\rangle$, that correspond to a change of basis, as

$$|\psi_i^A\rangle = \sum_j c_{ij}|j\rangle_A \tag{2.12}$$

$$|\psi_i^B\rangle = \sum_k d_{ij}|k\rangle_B, \tag{2.13}$$

we can apply the *Schmidt decomposition*

$$|\psi\rangle = \sum_i \sqrt{p_i}|\psi_i^A\rangle \otimes |\psi_i^B\rangle. \tag{2.14}$$

Then, let us say we can only access the information in the quantum system A. We would evaluate this information associated with the system A using the *reduced density matrix* ρ_A, defined as [41]

$$\rho_A = \mathrm{Tr}_B(\rho_{AB}) = \mathrm{Tr}_B(\sum_{i,j} \sqrt{p_i p_j}|i\rangle\langle j|_A \otimes |\tilde{i}\rangle\langle\tilde{j}|_B) \tag{2.15}$$

$$= \sum_{i,j,k} \sqrt{p_i p_j}|i\rangle\langle j|_A\langle k|\tilde{i}\rangle_B\langle\tilde{j}|k\rangle_B \tag{2.16}$$

$$= \sum_{i,j,k} \sqrt{p_i p_j}|i\rangle\langle j|_A\langle\tilde{i}|k\rangle_B\langle k|\tilde{j}\rangle_B. \tag{2.17}$$

This is most often seen written as

$$\rho_A = \sum_i p_i|i\rangle\langle i|_A. \tag{2.18}$$

As an example of entangled quantum system, let us consider a system of two spins. The state

$$A|\uparrow\rangle \otimes |\uparrow\rangle + B|\downarrow\rangle \otimes |\downarrow\rangle \tag{2.19}$$

is then entangled if neither of the coefficients, A or B, vanishes. Describing exactly how entangled the states are, boils down to the values of their amplitudes: if A and B have values close to each other, the state can be described as more entangled than the one with widely differing amplitudes. In other words, the entanglement of the state is equivalent on having uncertainty about the state. Evaluating the entanglement entropy is a way to measure the amount of this uncertainty. Now, it may be hard to evaluate the expectation value of the quantity that has a logarithm. For this reason, we can use the Rényi entropy to obtain our entanglement entropy. We start from the Rényi entropy

$$S_n = \frac{1}{1-n}\ln\sum_i p_i^n = \frac{1}{1-n}\ln\mathrm{Tr}(\rho^n) \tag{2.20}$$

and then take this to the limit of $n \to 1$. The resulting entanglement entropy is better known as the von Neumann entropy [51], defined for the density matrix ρ of the state:

$$S(\rho) = \langle -\mathrm{lg}(\rho)\rangle = -\mathrm{Tr}(\rho\mathrm{lg}\rho). \tag{2.21}$$

The entanglement entropy has proven to be extremely difficult to evaluate in the field theories, even without any interactions. However, if the field theory is at strong coupling, we can obtain the entanglement entropy using the holographic duality. This conjecture is known as the Ryu-Takayanagi proposal [44]. It gives information about the connection of entanglement on the boundary and bulk geometry by stating, that in holographic CFT, the entanglement entropy of a spatial region A can be given as

$$S(A) = \frac{\mathrm{Area}_{min}(\Sigma_A)}{4G_N}. \tag{2.22}$$

The left hand side in 2.22 represents the holographic entropy and the right hand side is the definition for it. In the last section, we discussed about how the field

theory lives on the boundary geometry. The Ryu-Takayanagi proposal 2.22 therefore describes how the holographic entanglement entropy $S(A)$ is determined from a surface that minimizes the Area(Σ_A). The Σ_A is a codimension-2 bulk surface, where the term codimension refers to the number of dimensions that can be removed from the submanifold. In other words, it refers to the dimension of the quotient space between the given vector space and its subspace. The codimension-2 bulk surface Σ_A is required to have the same boundary as A[3]. In addition, we require that Σ_A is anchored and homologous to A. In the figure 2, we have visualized a system with the geometry that is asymptotically AdS_{d+1}, where the holographic entanglement entropy can be evaluated with Ryu-Takayanagi proposal.

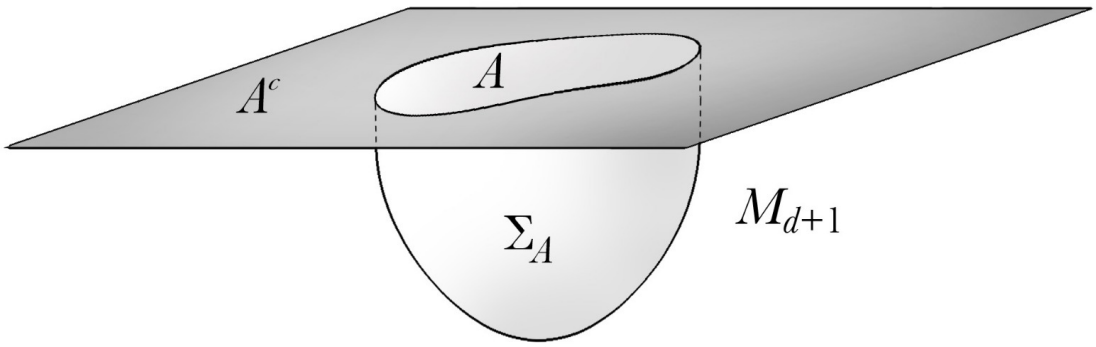

Figure 2: Visualization of the system for Ryu-Takayanagi proposal, where the entanglement entropy of A can be evaluated with the surface Σ_A.

If we consider a non-discrete case, the entanglement entropy is UV-divergent on the field theory side, which can be seen through the holography. Thus, to get rid of the divergence, cutoffs are required. Calculations of the entanglement entropy are thus required to be done with re-normalization of the action. In general, the pipeline for the entanglement entropy calculation starts from introducing the induced metric g_* on the surface Σ_A embedded in the bulk. Then, minimization of this surface allows us to use the Ryu-Takayanagi formula (2.22) to obtain the entanglement entropy. If the bulk metric is denoted by g and the embedding by f, then the induced metric is

$$g_* = f * g = \frac{\partial x^\alpha}{\partial y^\mu}\frac{\partial x^\beta}{\partial y^\nu} g_{\alpha\beta} dy^\mu \otimes dy^\nu. \tag{2.23}$$

Using g_*, we can obtain the area of Σ_A using its volume:

$$\mathrm{Vol}(\Sigma_A) = \int \sqrt{\det g_*}\, dy^1 \wedge \cdots \wedge dy^{d-1} \tag{2.24}$$

$$= \int \mathcal{L}(x(y), y) dy, \tag{2.25}$$

where $\mathcal{L}$ denotes the Lagrangian of the system. We can continue the calculation using the familiar Euler-Lagrange formulation

$$\frac{\partial \mathcal{L}}{\partial x^{\mu}(y)} - \frac{\partial}{\partial y^{\nu}}\left(\frac{\partial \mathcal{L}}{\partial(\partial_{\nu} x^{\mu}(y))}\right) = 0, \tag{2.26}$$

and minimize the action. Now, it is important that we consider the divergence of the area. Often, the divergence is bypassed by re-normalization, namely by considering a cutoff. This means that, at some $z = \epsilon$, we encounter the ending of the surface instead of encountering the ending at the boundary of AdS.

2.2 Entanglement wedge

Yet another holographic probe and a measure of entanglement for mixed states is the entanglement wedge and its cross section. If we consider a boundary region A of the AdS in terms of holography, the entanglement wedge itself is defined as the bulk domain of dependence of a surface that is bounded by Σ_A and A. Interestingly, it has been proposed that, the entanglement wedge can reach beyond its corresponding bulk region [6]. This can be stated in another way, by introducing a *causal wedge*, denoted by $\mathcal{C}_A$, that is the intersection between the causal future and causal past for the domain with dependence of A in the bulk. In terms of $\mathcal{C}_{\mathcal{A}}$, we can say that the Σ_A can reach beyond this causal wedge [52].

By considering a density matrix ρ_A, we reconstruct the entanglement wedge using this density matrix. In addition, we face an interesting feature of that we can find a larger system with pure state so that the density matrix of the mixed state is actually the reduced density matrix of this pure state. In other words, we can track down the original state by tracing partially over the states corresponding to the considered mixed states. This is called *purification*, and the reason it to be a particular interest for us, is that we can measure the entanglement of this purification. Now, when the purification is described via the Schmidt composition (2.14), we can define the entanglement of this purification, $E_P(A, B)$, as

$$E_P(\rho_{AB}) = \min_{\rho_{AB}=\mathrm{Tr}_{\overline{AB}}|\psi\rangle\langle\psi|} S(\rho_{A\overline{A}}), \tag{2.27}$$

where the two regions A and B are the two overlapping areas on the boundary. Marking the union of A and B as AB, we can refer to the entanglement wedge as M_{AB}. Then, we know that M_{AB} is associated with minimized surface Γ_{AB}. The purifications of ρ_{AB} are marked as the states $|\psi\rangle$ by using the definition

$$\rho_{A\tilde{A}} := \mathrm{Tr}_{B\tilde{B}}|\psi\rangle\langle\psi|, \tag{2.28}$$

in which the minimization has been done over all pure states $|\psi\rangle \in \mathcal{H}_{A\tilde{A}} \otimes \mathcal{H}_{B\tilde{B}}$. We must take into account that these pure states must satisfy the following condition:

$$\rho_{AB} = \mathrm{Tr}_{\tilde{A}\tilde{B}}|\psi\rangle\langle\psi|. \tag{2.29}$$

In other words, the states $|\psi\rangle$ that satisfy (2.29) are the purifications of the ρ_{AB} [46].

2.2.1 Entanglement wedge cross section

The entanglement of the purification has a candidate gravity dual, which is the entanglement wedge cross section [48]. Therefore, we can write them as

$$E_p(\rho_{AB}) = E_W(A, B). \tag{2.30}$$

To explain more detail how this description is realized, we take a look at the entanglement wedge M_{AB}. For certain M_{AB}, we may consider a case where it is connected and contains subregions A and B. In this situation, we find that the boundary of ∂M_{AB} can be further divided into the parts corresponding to the regions A and B [41] as

$$\partial M_{AB} = A \cup B \cup \Gamma_{AB}, \tag{2.31}$$

where the Γ_{AB} is the minimal surface associated to the entanglement wedge. Furthermore, it can be presented in terms of the minimal areas of the individual regions:

$$\Gamma_{AB} = \Gamma_{AB}^{(A)} \cup \Gamma_{AB}^{(B)}. \tag{2.32}$$

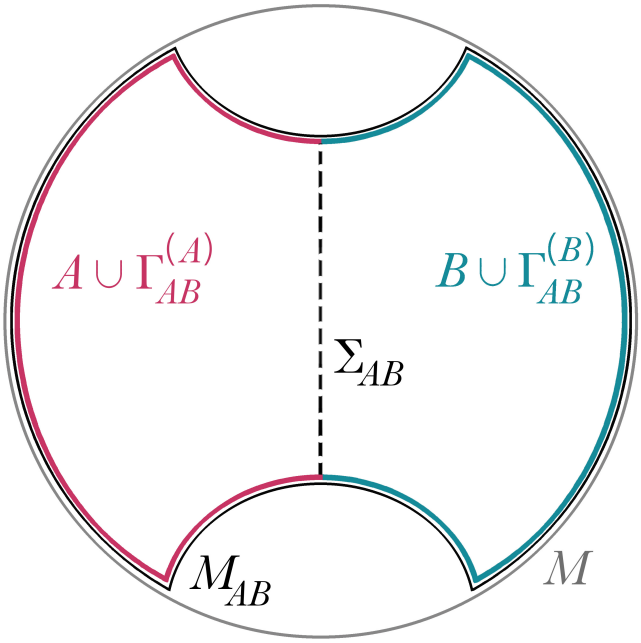

Figure 3: Graphical visualization of the entanglement wedge and its regions $A \cup \Gamma_{AB}^{(A)}$ and $B \cup \Gamma_{AB}^{(B)}$ that encounter each other at $\partial\Sigma_{AB}$, meaning that the minimization of the surface Σ_{AB} is the corresponding entanglement wedge cross section.

If we now take a look at the area where our regions $A \cup \Gamma_{AB}^{(A)}$ and $B \cup \Gamma_{AB}^{(B)}$ encounter each other and call this area Σ_{AB}, we can arrive at the definition of the *entanglement wedge cross section*. A visualization of entanglement wedge cross

section E_W is presented in the Figure 3. It is defined as the minimal area of the surface Σ_{AB}

$$E_W(\rho_{AB}) = E_W(A, B) = \frac{\text{Area}(\Sigma_{AB}^{\min})}{4G_N}, \tag{2.33}$$

where ρ_{AB} is a density matrix that the purification is performed on. Indeed, the discussed entanglement of the purification is dual to the entanglement wedge cross section [47]. Thus, E_W yields a way of obtaining information about the correlation measure without having to evaluate the entanglement of the purification itself. It hands us the information about the correlation of A and B via their union $A \cup B$ that corresponds to the density matrix of the associated mixed state ρ_{AB}. We shall return to the discussion of the entanglement wedge cross section in the later chapters.

While we chose to concentrate on the entanglement wedge cross section as the dual for the entanglement of purification, it is not the only possible dual. For example, *entanglement negativity* is one proposal [28]. It has been suggested that the entanglement negativity is, in fact, a dual for the entanglement wedge cross section [31].

2.2.2 Odd and reflected entropies

A question worth asking is if the entanglement wedge cross section could be obtained directly from the given state. This question has been answered affirmative with the introduction of odd and reflected entropies. The key notation with these two is that they are in fact simple refinements on E_W. This means that with additional assumptions, the calculation of the entanglement wedge cross section can be simplified by the calculation of associated entropy. The first of these two refinements, the odd entropy, is proposed as an odd integer analytic continuation of Tsallis entropy. The Tsallis entropy for discrete cases is originally defined as

$$S_T = \frac{k}{q-1}\left(1 - \sum_i p_i^q\right), \tag{2.34}$$

where the p_i are the discrete probabilities that sum up to one, the q is a real parameter and k is positive constant [50]. The odd entropy S_0 is the analytic continuation of (2.34), for the odd integer $n_0 \to 1$ by Tamaoka et al. [47]:

$$S_0(\rho_{A_1A_2}) = \lim_{n_0 \to 1} S_0^{(n_0)}(\rho_{A_1A_2}). \tag{2.35}$$

Moreover, it was proved that (2.35) reduces to the entanglement entropy for ρ_{A_1} in case of a pure state and that (2.35) reduces to the von Neumann entropy in case of product state. In addition, Tamaoka et al. demonstrate a calculation of $S_0(\rho_{A_1A_2}) - S(\rho_{A_1A_2})$ in two dimensions, obtaining

$$S_0(\rho_{A_1A_2}) - S(\rho_{A_1A_2}) \equiv \mathcal{E}_W(\rho_{A_1A_2}) = E_W(\rho_{A_1A_2}). \tag{2.36}$$

Here the $\mathcal{E}_W$ is defined through $\mathcal{E}_W = S_0(\rho_{A_1A_2}) - S(\rho_{A_1A_2})$. The equation 2.36 states, that the difference between the odd entropy $S_0(\rho_{A_1A_2})$ and the von Neumann entropy

$S(\rho_{A_1A_2})$ yields the entanglement of purification E_P, which is the holographic dual of entanglement wedge cross section E_W.

Another refinement is the so called reflected entropy. It was introduced in [15] via considering reflected minimal surfaces and obtaining the entanglement entropy from them. For entanglement wedge E_W with regions A and B, they conjectured that the reflected entropy on the continuum limit to be

$$S_R(A,B) = 2E_W(A,B). \tag{2.37}$$

To understand this result, we need to add few notes about the states and spaces behind it. First, we can relate it to the AdS deconfining geometry, which describes the black hole. In that case, we have a situation where the entanglement wedge is in fact anchored to A and A^* where $A^* = JAJ$, and J is an anti-unitary CPT (charge, parity, time). A visualization of such a situation is presented in Figure 4. A crucial assumption in the calculation of the reflected entropy is that the considered QFT satisfies the split property. Namely, it means that the algebra describing the QFT can be further splitted into subalgebras. These subalgebras correspond to space-like separated regions which are associated to independent states. By assuming such a QFT let us introduce a $\mathcal{N}$ that is the factor performing the splitting of the algebras, i.e.

$$\mathcal{A}_A \subset \mathcal{N} \subset \mathcal{A}'_B. \tag{2.38}$$

Here $\mathcal{A}_A$ is a subalgebra of the algebra for our region B and $\mathcal{A}'_B$ represents the commutant of the same algebra of B.

Now, to fully bring together all the important properties this splitting factor must satisfy, we need to become familiar with some concepts of the von Neumann algebra. In general, the factors in this algebra refer to algebra with identity operator multiples in the center. There are three different types we can divide these factors into. For type I factors, there is nonzero minimal projection. For type II, there does not exist minimal projections at all but instead, there are finite-projections. These are nonzero projections that can be divided further into the sum of two projections. For type III factors, there are no nonzero finite projections. Using this information, the conjecture of [15] becomes more clear: they demand the factor $\mathcal{N}$ that splits the algebras to be type I factors and canonical. Of a given state ψ and $\mathcal{N}$ splitting the algebras of the space-like separated regions A and B, the reflected entropy S_R in the continuum limit is

$$S(\mathcal{N}) = 2E_W(A,B) + \mathcal{O}(G_N^0). \tag{2.39}$$

Here the correction term is the first quantum correction in the expansion with respect to G_N: The first term is the one that is already coefficient to the entanglement wedge. We shall now drop the correction term, and continue with only the first term. Yet another way of presenting the S_R is with the associated density matrix. For the density matrix $\rho_{AA^*BB^*} = |\sqrt{\rho_{AB}}\rangle\langle\sqrt{\rho_{AB}}|$, the reflected entropy is obtained by tracing over subsystems and arriving at

$$S_R(A,B) := S(AA^*)_{\sqrt{\rho_{AB}}} = S(BB^*), \tag{2.40}$$

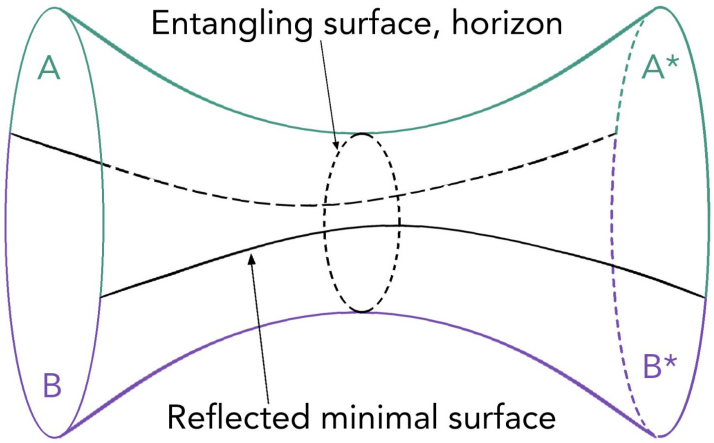

Figure 4: For AB, that is a Hilbert space, the horizon can be treated as the entangling surface. The area of this RT surface is twice the minimal E_W.

where again, $A^* = JAJ$ and the purification is presented with

$$\rho_{AB} = \mathrm{Tr}|\sqrt{\rho_{AB}}\rangle\langle\sqrt{\rho_{AB}}|. \tag{2.41}$$

The reflected minimal surface used to obtain the reflected entropy is visualized in Figure 4 via the separated regions A and B and their entanglement wedge cross section.

These results hold for QFTs with holographic duals that the split property applies to when quantized on the manifold. One relatively recent discussion on this assumption within holography is presented in [22]. Furthermore, one might ask, does the reflected entropy satisfy the set of inequalities that the entanglement entropy does. There are a few inequalities particularly interesting for the reflected entropy. The first one is

$$S_R(A : BC) \geq I(A : B) + I(A : C), \tag{2.42}$$

which has been proven to hold in holography [15], since for mutual information satisfies the inequality (1.15), the (2.42) follows from the inequality of

$$S_R(A : BC) \geq I(A : B). \tag{2.43}$$

The second one is

$$S_R(A : BC) \geq S_R(A : B), \tag{2.44}$$

which has received failed attempts of proof due to the entanglement wedge cross section being related to the entanglement wedge nesting. This in part produces complications on the calculation of the correlation functions with modular flow. The third inequality proposed for the reflected entropy following the strong superadditivity is

$$S_R(A_1A_2 : B_1B_2) \geq S_R(A_1 : B_1) + S_R(A_2 : B_2), \tag{2.45}$$

with proposed proof by [15]. In more detail, their fundamental conjecture is that for the algebra splitting factor $\mathcal{N}$, the entanglement wedge is UV-finite since the boundary of AdS is not reached. Thus, the calculation of the entropy reduces to calculation of the area of the reflected minimal surfaces. Indeed, the reflected entropy as a measure of correlation between A and B is considered over other such measures due to its relatively simple formulation.

In addition to odd and reflected entropies, there is yet another method considered useful with the calculation of the entanglement wedge cross section. It is introduced by Harper and Headrick [23], where they use the *bit threads formalism* to generate a flow formulation for the entanglement wedge cross section. In the framework of holography, we can study the probes such as entanglement entropy either with the extremal surfaces, as we have discussed so far, but with bit threads. The bit threads are vector fields that have a bound norm and do not have divergence. The norm bound is obtained from the Planck length. We can think them as curves that have transverse density equal to the norm of the vector field everywhere. In addition, the threads can only end on the boundary of the manifold. A major reason the extremal surfaces are used is the non-locality of the information about the metric. However, there are examples cases that introduce choices of bit threads that exploits the locality of the bulk [1]. One example of this is a proposal by Freedman and Headrick for the calculation of the entanglement entropy by not relying on the bulk surface but flow minimization instead:

$$S_A = \frac{1}{4G_N}\max_{v\in\mathcal{F}}\int_A \sqrt{h}n_\mu v^\mu. \tag{2.46}$$

Here

$$\mathcal{F} = \{v|\nabla_\mu v^\mu = 0, |v| \leq 1\}$$

and A is defined as the boundary of minimal surface on our manifold. The flow is a vector field v on the manifold. It has no divergences and satisfies $|v| \leq \frac{1}{4G_N}$ [11]. In (2.46), $\sqrt{h}$ is square root of the determinant of the induced metric. This form of entanglement entropy can be shown to be equal to the Ryu-Takayanagi formula (2.22) through the Riemannian max flow and min cut theorem. In fact, it was proven that if we consider a minimal hypersurface $m(A)$ located in the bulk, the area of that surface is equal to the maximum flow that comes out from the region A [18][25]. This requires the boundary region A to be optimized over all those vector fields in the bulk that have no divergence. This means that, the entanglement entropy can be written using the max flow as

$$S(A) = \max_{v \text{ flow}}\int_A v. \tag{2.47}$$

Then, the equivalence is recovered via the Riemann max flow-min cut theorem as

$$\max_{v \text{ flow}}\int_A v = \frac{1}{4G_N}\min_{v \text{ flow}}\text{Area}(m(A)), \tag{2.48}$$

where $m(A)$ is the minimal surface with boundary A.

The main difference between the flow-based entropy and the RT-entropy is that the minimized surface is typically unique, but the result of max flow theorem is highly degenerated. Indeed, there are questions to address relating this alternative method of reconstructing the metric of which few such question Agon et. al [1] discuss in their publication.

2.3 Correlation functions

To detect the correlation between probes, we must evaluate the *correlation functions*. The usefulness of them is that in the case of the considered systems being independent from one another. This relates to the mutual information (1.14), where we obtain zero in the case of independent systems. In the framework of field theory, the correlation functions are sometimes referred to as Green functions, in the case where our correlation function is a 2-point function. This goes back to the free field theory where the correlation function of differential operator is in fact the Green function. The correlation functions are also known as the n-point functions, and defined as

$$\langle \mathcal{O}(x_1) \dots \mathcal{O}(x_n) \rangle = \frac{\int \mathcal{D}\phi e^{-S[\phi]} \phi(x_1)\phi(x_2)\dots\phi(x_n)}{\int \mathcal{D}\phi e^{-S[\phi]}} \tag{2.49}$$

$$= \frac{\delta^{(n)} S^{\text{renorm.}}_{\text{grav.}}[\phi]}{\delta\varphi(x_1)\dots\delta\varphi(x_2)}, \tag{2.50}$$

where $S^{\text{renorm.}}_{\text{grav.}}[\phi]$ is the renormalized version of the on-shell gravity action [33]. Calculations of the n-point functions is often done in the momentum space due to better understanding of the behavior of the divergence at $p \to \infty$. The case we are particularly interested in is the two-point function. For a scalar field ϕ it is defined as

$$G_E(x-y) = \langle \mathcal{O}(x)\mathcal{O}(y) \rangle. \tag{2.51}$$

However, as discussed, we prefer to work in the momentum space and thus transform (2.51) into momentum space by introducing $\langle \mathcal{O}(x) \rangle_\varphi$ as the path integral of one-point function with source φ. It measures the amount of fluctuation of our probe from the expectation value. By expanding this into power series within linear order, we can write $\langle \mathcal{O}(x) \rangle_\varphi$ as

$$\langle \mathcal{O}(x) \rangle_\varphi = \int d^d y G_E(x-y)\varphi(y). \tag{2.52}$$

With this, the expression for the two-point function for normal-ordered probe (i.e. $\langle \mathcal{O}(x) \rangle_\varphi$ vanishes) in momentum space becomes

$$G_E(k) = G_E(k)\varphi(k). \tag{2.53}$$

To bring this more related to the calculation of the action, the two point function is evaluated with the on-shell action. Considering a case of scalar field ϕ , we can write

$$S^{\text{on-shell}} = -\frac{\nu}{2} \int dz d^d x \partial_M [\sqrt{g}\phi_M g^{MN} \partial_N \phi], \tag{2.54}$$

that with the boundary at $z = \epsilon$ reduces to

$$S^{\text{on-shell}} = \frac{\nu}{2} \int d^d x (\sqrt{g} \phi g^{zz} \phi)_{z=\epsilon}. \tag{2.55}$$

Once again, we note that there is divergence in the action. The reasonable way to get rid of it is to define a quadratic term on the boundary of our AdS and add it to the on-shell action to bypass the divergence. A proper term to use would be

$$\int_{\partial AdS} d^d x \sqrt{\det(\gamma_{\mu\nu})} \phi^2(\epsilon, x), \tag{2.56}$$

where $\gamma_{\mu\nu}$ is the induced metric:

$$ds^2_{z=\epsilon} = \gamma_{\mu\nu} dx^\mu dx^\nu = \frac{R^2}{\epsilon} \delta_{\mu\nu} dx^\mu dx^\nu. \tag{2.57}$$

2.4 Wilson loops

One of the most important probes are the Wilson loops. Most often, they are defined as

$$W_C := \text{Tr} \left(\mathcal{P} \exp \left(i \oint_C A_\mu dx^\mu \right) \right), \tag{2.58}$$

where $\mathcal{P}$ is a path-ordering operator, mainly used as time-ordering operator $\mathcal{T}$. They are probes through the holonomy of the gauge field A_μ introduced previously through Yang-Mills theory. For a particle on a given manifold with connection A_μ that is parallel transported along the closed loop C, we actually have an effect analogous to the so called *Aharonov-Bohm effect*. This effect describes how particle is affected by A_μ through the phase factor and thus introducing the phase as a probe, creating a phase factor for the wave function of the particle. Thus, the Wilson loops are really phase factors in gauge theories and they are expressed as the trace of a path-ordered exponential for A_μ along closed loop C.

The Wilson loop can be obtained from string theory as an invariant action for our string [49]. In holography, the expectation value of the Wilson loop is the most informative, since it relates to the partition function of the string:

$$\langle W_C \rangle = \int \mathcal{D} X^\mu e^{-S_{NG(\Sigma)}}, \tag{2.59}$$

where the path integration is to be done over the worldsheet coordinates and S_{NG} is the action which we will introduce later in this section. In the limit of strong coupling, one can perform a saddle point approximation to this expression and obtain the reduced form [17]:

$$\langle W_C \rangle = e^{-S_{NG(\Sigma)}}. \tag{2.60}$$

In the Figure 5, the set up for Wilson loop is visualized through holography. We may think the closed loop as the boundary that a fundamental string hangs from.

Furthermore, the potential energy between antiquark and quark results from the calculations of the equations of motion for this string:

$$V_{q\bar{q}} = S_{NG} - S_{NG}^{||}, \tag{2.61}$$

where the action $S_{NG}^{||}$ is of the free string.

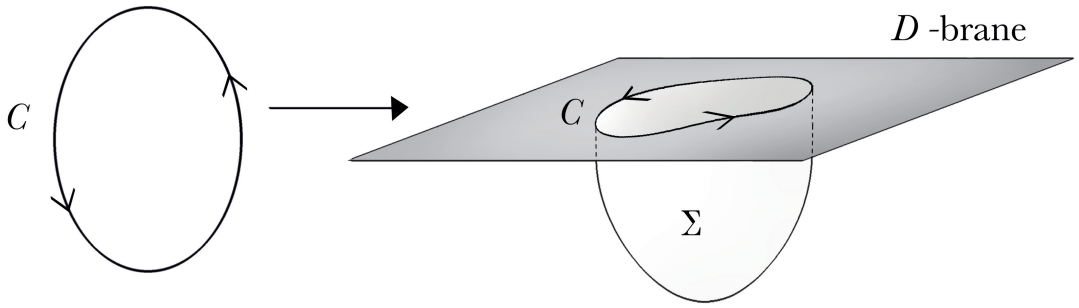

Figure 5: Visualization of the holonomy of the gauge connection through which the Wilson loops are defined. In terms of holography, the Wilson loop along curve C can be then presented as the boundary of Σ lying on the D-brane.

Now, in order to carry out the calculations of Wilson loops, we need to introduce and evaluate the needed action. In this case, we can consider a case where the string has ending in the boundary of AdS and then embed this string. We obtain the induced metric that is then used to calculate the on-shell Nambu-Goto action *Nambu-Goto action*. In general, when the induced metric is written as

$$g_{\alpha\beta} = \eta_{\mu\nu} \frac{\partial X^\mu}{\partial \tau} \frac{\partial X^\nu}{\partial \sigma}, \tag{2.62}$$

and the determinant of the metric is introduced as

$$\det(g_{\alpha\beta}) = (\frac{\partial X}{\partial \tau})^2 (\frac{\partial X}{\partial \sigma})^2 - (\frac{\partial X}{\partial \tau} \cdot \frac{\partial X}{\partial \sigma})^2 \tag{2.63}$$

, we can arrive at a result where the action is proportional to the worldsheet:

$$S_{NG} = -T \int d^2\sigma \sqrt{-\det(g_{\alpha\beta})}, \tag{2.64}$$

where T denotes the proportionality constant, and in more detail it is the tension of the string. Now, by plugging in the metric, we obtain the Nambu-Goto action as

$$S_{NG} = -T \int d^2\sigma \sqrt{(\frac{\partial X}{\partial \tau})^2 (\frac{\partial X}{\partial \sigma})^2 + (\frac{\partial X}{\partial \tau} \cdot \frac{\partial X}{\partial \sigma})^2} \tag{2.65}$$

which can be expressed as

$$S_{NG} = -T \int d^2\sigma \sqrt{-\dot{X}^2 X'^2 + (\dot{X} \cdot X')^2}. \tag{2.66}$$

For coordinates $X^\mu = (t, \vec{x})$ at certain time when $\frac{d\vec{x}}{d\tau} = 0$, this can be interpret as integration over the spatial length of the string. The action has fundamentally two symmetries: First one to mention is the Poincaré invariance, namely that the transformation parameters do not depend on the coordinates on the worldsheet. Second one is the re-parametrization invariance, which can be described as gauge symmetry.

Speaking more generally, we can link the Wilson loops to the electric operators in which case, the S-duality results in mapping these Wilson loops to their magnetic counterparts. These are naturally the magnetic ones called *'t Hooft loops*, which we will introduce and discuss in detail in the next section.

2.5 't Hooft loops

The holographic calculation of the 't Hooft loops follows the same pattern as the Wilson loops. However, instead of the already familiar Nambu-Goto action for the Wilson loops, we consider a D1-brane action in string theory. The difference of 't Hooft loops to the Wilson loops arises as we need to take the dilaton into account and thus evaluate the action as

$$S_{D1} = -\tilde{T} \int d^2\xi e^{-\phi} \sqrt{-\det(g_{\alpha\beta})}, \tag{2.67}$$

where $\tilde{T}$ is the tension for a $D1$-brane, ϕ stands for the dilaton and ξ are the coordinates of the D1-brane. When minimizing this action, result yields the loop we are interested in.

Notice that, if we wish to work with the mentioned $\mathcal{N} = 4$ SYM theory, the 't Hooft loop reduces to version that is analogous to the Wilson loop, since the dilaton is constant in the $\mathcal{N} = 4$ SYM theory. This comes from the the dilaton being dual to the coupling constant. This means that, 't Hooft loops differ from Wilson loops only in field theories with non-trivial coupling constants, corresponding to radially depending dilaton fields in the bulk.

However, there are some additional and interesting points about the 't Hooft loops even in the $SU(N)$ $\mathcal{N} = 4$ Yang-Mills theory. The discussion of 't Hooft loops can be further taken to include the discussion about S-duality and the supersymmetry of these loops. Recalling that through the gauge connection our loop operators can be determined to conserve some amount of supersymmetry. This connection with the scalar fields corresponds to the Bogomol'nyi–Prasad–Sommerfield (BPS) operators in case where annihilation between them and fermion field Ψ. In detail, it means that for fermion field Ψ with field strength F_{MN}, the solution of scalars ϕ is [40]

$$\phi(y)^A = \frac{\lambda}{2\pi} \int ds \frac{\theta^A(s)}{(y - x(s))^2}. \tag{2.68}$$

The condition we require for the BPS operator is

$$\delta\Psi = \frac{1}{2}\Gamma^{MN} F_{MN}\epsilon - 2\Gamma^A \phi^A \epsilon_1 = 0. \tag{2.69}$$

Here $\epsilon = \epsilon_0 + x_\mu \Gamma^\mu \epsilon_1$ with ϵ_0 and ϵ_1 being the Majorana-Weyl constant spinors and $A = 4, \ldots, 9$ and $M, N = 0, \ldots, 9$ as in the regular ten dimensional notation. The Γ:s present the usual gamma matrices with Clifford algebra $C\ell_{1,3}(R)$. Then, we can consider the variation of the Ψ and the use of the identity

$$\epsilon_{\mu\nu\rho\sigma}\Gamma^{\rho\sigma} = -2\Gamma^{\mu\nu}\Gamma^{1234}, \tag{2.70}$$

to get rid of the Levi-Civita tensor in the variation of Ψ. Then, the condition for supersymmetry reduces and gives our operator the desired BPS nature in terms of the circular path $x_\mu(s)$ and the couplings $\theta^A(s)$ that are scalar:

$$\delta\Psi = \oint ds\left(\frac{(y-x)_\mu \Gamma^\mu}{(y-x)^4}[i\Gamma^\nu \cos\phi \dot{x}_\nu + \Gamma^{1234}\Gamma^\nu \sin\phi \dot{x}_\nu + \Gamma^A \theta^A](\epsilon_0 + \Gamma^\nu x_\nu \epsilon_1)\right) \tag{2.71}$$

$$= 0. \tag{2.72}$$

This is zero when the integrand is zero. Furthermore, for electric loop ($\phi = 0$) this reduces to the condition of Maldacena-Wilson operator and thus gives us the condition for the regular (BPS) Wilson loops:

$$[i\Gamma^\mu \dot{x}_\mu + \Gamma^A \theta^A](\epsilon_0 + \Gamma^\nu x_\nu \epsilon_1) = 0. \tag{2.73}$$

Now, in the case of 't Hooft operator and loops, we consider the gauge group as $G = U(N)$, and define a homomorphism map as

$$\rho : U(1) \to G, \tag{2.74}$$

which for the exponential $e^{i\alpha} \in U(1)$ gives mapping of

$$G = e^{i\alpha B} = \mathrm{diag}(e^{im_1\alpha}, \ldots, e^{im_N\alpha}), \tag{2.75}$$

in which we take m_i to be the magnetic weights of the G, i.e. vectors that identify the irreducible representation of this group. We can then define the 't Hooft operator in a certain representation of G with either k-symmetry of antisymmetry so that the matrix B is

$$B_{k-symm.} = \mathrm{diag}(\underbrace{k, 0, \ldots, 0}_{N}) \tag{2.76}$$

$$B_{k-antisym.} = \mathrm{diag}(\underbrace{1, 1, \ldots, 1}_{k}\underbrace{0, \ldots, 0}_{N}). \tag{2.77}$$

Using this, we get the conditions for our operator very similar to the Abelian case, but modified to include the diagonal matrix B as

$$A_\mu(y) = B\int ds \frac{\dot{x}(s)}{(y - x(s))^2}, \tag{2.78}$$

$$\phi^A(y) = B\int ds \frac{\theta^A(s)}{(y - x(s))^2}, \tag{2.79}$$

and then obtain the condition after variation for non-Abelian case similarly to previous one as

$$\delta_\epsilon \Psi = \frac{1}{2}\Gamma^{MN} F_{MN}\epsilon(s) - 2\phi^A \Gamma^A \epsilon_1 = 0. \tag{2.80}$$

Let us now consider the circular motion and finally get to the actual, circular 't Hooft loops. Starting with

$$x_\mu(s) = (\cos(s), \sin(s), 0, 0), \tag{2.81}$$
$$\theta^A(s) = \theta_0^A, \tag{2.82}$$

and continuing to the configurations introduced in (2.68) via mapping of $\mathbb{R}^4$ to the $AdS_2 \times S_2$ gives

$$\phi^A(y) = 2\pi B \frac{\theta_0^A}{\sqrt{(1+y^2)^2 - 4(y_1^2 + y_2^2)}}. \tag{2.83}$$

After this, performing the variation of the 't Hooft operator results in the condition for circular BPS 't Hooft loop:

$$(\Gamma_{\epsilon_1}^{34} + \Gamma^A \theta_0^A \epsilon_0) = 0. \tag{2.84}$$

Similarly to the Wilson loop, this circular 't Hooft loop preserves half of the supersymmetries. As mentioned earlier, the expectation value of 't Hooft loop is analogous to the expectation value of the Wilson loop,

$$\langle H \rangle = e^{-S_{D1}}. \tag{2.85}$$

Recall, that the vacuum expectation value of the 't Hooft loop differs from that of the Wilson loop if the coupling of the theory is not constant in energy. In the bulk, this difference manifests itself through a non-trivial dilaton field entering explicitly in the D1-brane action (2.67), absent in the Nambu-Goto action (2.66).

Another note to add in the discussion of 't Hooft loops is in the large-N QCD, where the propagator of quark field and belonging to the group $SU(N)$, obeys

$$\langle \psi_i \overline{\psi_i} \rangle \propto \delta_{ij}. \tag{2.86}$$

Here the propagation happens from i to j, namely marked with the color indices. Let us consider taking N large [32][33][19], which is known as the 't Hooft limit. The $SU(N)$ algebra itself has generators that give the propagator components expressed above to be proportional to $\delta_l^i \delta_j^k - \delta_j^i \delta_l^k / N$, which corresponds to propagation of gluons. Hence, the large N limit in this association is equivalent with neglecting the term with N. Generally speaking, taking the 't Hooft limit helps to simplify the QCD by concentrating the dynamics only to the planar diagrams [30].

Furthermore, the *'t Hooft coupling* is encountered with the large N limit, namely the limit of large numbers of colors. In detail, this is the coupling of

$$\lambda = g_{YM}^2 N_c \tag{2.87}$$

with fixed λ that satisfies $\lambda \gg 1$. The limit $N_c \to \infty$ is then the limit of large N_c. Interestingly, in this theory with topologically invariant Euler characteristics ξ, the partition function is in fact given by the sum of topologies from the 2-dimensional surfaces associated [38], i.e.

$$\ln Z_{\text{gauge}} = \sum_{i=0}^{\infty} N_c^{\xi} f_i(\lambda). \tag{2.88}$$

This marks the connection to the holographic duality, where we can see the similarity of the partition functions between the string and gauge theories.

3 EE inequalities

3.1 Fundamental inequalities

Earlier, in the Chapter 2.1, we discussed and introduced the entanglement entropy (EE) in the holography. The holographic entanglement entropy is useful not only in the calculation of dual probes in the bulk but also key to the mutual information of the system. It is important to note how entanglement entropy itself must satisfy some inequalities in order for the considered quantum state to be counted as holographic. Therefore, we will now introduce few of the most important inequalities of the entropy. Earlier, we introduced the von Neumann entropy. For that, we require the following inequality to be satisfied:

$$S(\rho) \geq 0. \tag{3.1}$$

This means that the entropy associated with the state density matrix ρ is always non-negative. The state for which the entropy is equal to zero is the pure state. In addition, the *strong subadditivity* is one of the most essential and well-known inequalities of entanglement entropy. This is considered when we have three regions A, B and C that are separated from one another. For their entropies, the strong subadditivity condition reads

$$S(AB) + S(BC) \geq S(B) + S(ABC), \tag{3.2}$$

where we have chosen to continue with shorter notation of marking the entropy $S(\rho_A)$ associated with density matrix ρ_A by writing it as $S(A)$. Similar short hand notation we used above is to write the entropy of an union $S(A:B)$ as $S(AB)$.

Yet another inequality is the monogamy inequality of the mutual information (1.15). We already encountered this in the discussion of the entanglement wedge. We can further write it for tripartite information as [7]

$$I(A:BC) \geq I(A:B) + I(A:C) \tag{3.3}$$

$$\Leftrightarrow I(A:BC) - I(A:B) - I(A:C) \geq 0. \tag{3.4}$$

Presented for any disjoint regions A, B and C [24][5]. The inequality is visualized with schematics in the Figure 6.

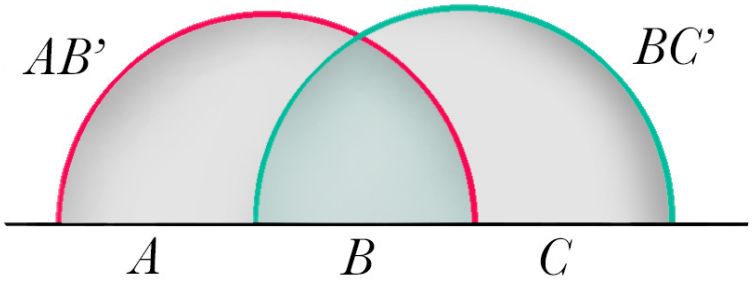

Figure 6: Visualization of the strong subadditivity. The gray regions correspond to the joint region of ABC, whereas the light blue region is the region B. When visualized, it becomes even more apparent that the proof of strong subadditivity is, after all, simply a geometrical proof.

If we have the system where the strong subadditivity is not applicable due to the number of regions being only two, we encounter the *subadditivity* inequality. This is analogous to the strong subadditivity with one of its three regions missing:

$$S(A) + S(B) \geq S(AB). \tag{3.5}$$

Finally, if we encounter system that is bipartite, we have to consider the inequality of

$$S(AB) \geq |S(A) - S(B)|, \tag{3.6}$$

which is known as the *Araki-Lieb inequality*. This inequality lets the entropies associated with the given subsystems to have larger values than the entropy of the system they together compose.

These inequalities are heavily used in the holographic context as well. They can be proved to work in the holographic formulation of the entanglement entropy. For example, the monogamy inequality 3.3 was originally proved for the Ryu-Takayanagi proposal in [26]. The strong subadditivity in the context of holography is proven in the [5], but as the number of regions is increased, the number of inequalities the RT-entropies must satisfy rises towards infinity. In the following chapters, we shall take more detailed look into the holographic entanglement entropy and the inequalities in the context of subregion duality.

3.2 Subregion duality

An essential concept in this context is the *subregion duality* that describes the duality between the entanglement wedge and the reduced CFT state of the boundary region. It answers to the question of whether there is a bulk region with full information corresponding to a boundary subregion that we have full information of. The subregion duality introduces entanglement wedge of the given boundary subregion as such object. In other words, the entanglement wedge has the information about the associated bulk state. Originally, the existence of such subregion duality was suspected due to the AdS/Rindler reconstruction [20]. For the causal wedge C_A for

the boundary subregion A, this construction solves the equations of motions using perturbations, resulting in the equations for operator in the CFT. This allows the field theory to model the effective field theory for the bulk in this causal wedge. But as the RT entropy proposes, the causal wedge is not the full story. It has been stated [6] that there are cases where the density matrix of the given boundary subregion would access the information from beyond the C_A. However, this would be in contradiction with the proposal of entanglement wedge reconstruction conjecture [27]: For the entanglement wedge $\mathcal{E}_A$, the theorem states that for

$$C_A \subseteq \mathcal{E}_A, \tag{3.7}$$

we can reconstruct the operators associated with the bulk via the entanglement wedge as field theory operators in the boundary subregion.

Since we are already familiar with the entanglement wedge cross section and the purification from Chapter 2, we can consider the associated inequalities. The entanglement of purification E_P (2.30) satisfies the following inequalities, proven by [48]:

$$\frac{1}{2}I(A:B) \leq E_P(A,B) \leq \min[S(\rho_A), S(\rho_B)], \tag{3.8}$$

$$E_P(\rho_{AB}) \leq E_P(\rho_{A(BC)}), \tag{3.9}$$

$$E_P(\rho_{A(BC)}) \geq \frac{1}{2}I(A:B) + \frac{1}{2}I(A:C). \tag{3.10}$$

where $I(A:B)$, defined in (1.14), stands for the mutual information for regions A and B [4]. Furthermore, we shall introduce the requirements for the corresponding entanglement wedge cross section. Naturally, we require $E_W(A,B) > 0$ since $\text{Area}(\Sigma_{AB}) \geq 0$. Furthermore, due to the duality to the entanglement of purification, entanglement wedge cross section must satisfy

$$E_W(A,B) \geq \frac{1}{2}I(A,B). \tag{3.11}$$

If we consider how the states are constructed, we arrive at vanishing E_W for the product state and $E_W(A,B) = \rho_{AB}$ for the pure state.

3.3 The holographic entropy cone

In [8], Bao et al. present a parametrization of the phase space constructed from the RT-entropies for a given CFT and call this parametrization as *holographic entropy cone*. The cone is constructed from the set of inequalities the RT-entropies satisfy, and visualized in Figure 7. Using this cone, they are able to find a complete set of inequalities for 2 to 4 regions, which is something that in general has not been done for arbitrary quantum systems. It has been known [13] that for 5 or more regions, the set of inequalities is infinite, and they claim to have found a new, infinite family of such inequalities. The most interesting aspect of their conjecture is the finite number of the inequalities for the regions with less than 5 regions. Their approach

for the finite set of inequalities for four regions is done with so called graph model that re-defines the RT-entropies as combinatorial problem and thus gives the number of ways to cut and reassemble the entanglement surfaces to new surfaces. By doing so, it restricts the entanglement entropies of other regions in the bulk.

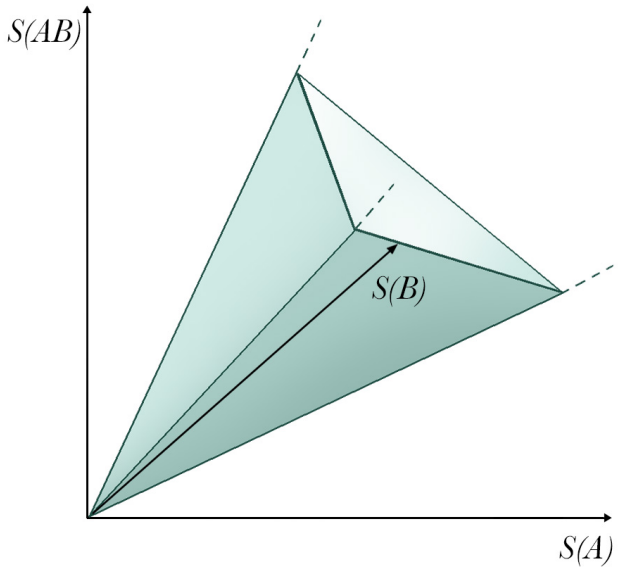

Figure 7: Graph showing the entropy cone for regions A and B. For two regions, there is only one extreme ray.

These minimal cuts, W_l, defined as

$$W_l := \bigcup \{W(x) : x \in \{0,1\}^L \text{ with } x_l = 1\} \tag{3.12}$$

are thought as the I_l-cuts for regions I_l with bitstrings $x_l \in \{0,1\}^L$. Furthermore, starting from a general inequality for the entropies from combinatorics

$$\sum_{l=1}^{L} \alpha_l S(I_l) \geq \sum_{r=1}^{R} \beta_r S(J_r), \tag{3.13}$$

they define a bulk inequality for these minimal cuts as

$$\sum_{l=1}^{L} \alpha_l |C(W_l)| \geq \sum_{r=1}^{R} \beta_r |C(U_r)|, \tag{3.14}$$

in which the cut of each region I_l is defined as the reassembling of the subset $\cap_{l=1}^{L} W_l^{x_l}$. Note that the bitstrings and their indices follow

$$x_i := (i \in I_l)_{l=1}^{L} \in \{0,1\}^L, \tag{3.15}$$

$$y_i := (i \in J_r)_{r=1}^{R} \in \{0,1\}^R, \tag{3.16}$$

where L and R are the total number of considered bitstrings x and y, respectively. By setting $S^*(I_l) = |C(W_l)|$ and assuming that the reassembling results in a new cut U_r as

$$U_r := \bigcup \{W(x) : x \in \{0,1\}^L \text{ with } f(x)_r = 1\} \tag{3.17}$$

for some function f, they show that in fact, the (3.14) satisfies the entropy inequality:

$$\sum_{l=1}^{L} \alpha_l S^*(I_l) = \sum_{l=1}^{L} \alpha_l |C(W_l)| \geq \sum_{r=1}^{R} \beta_r |C(U_r)| \geq \sum_{r=1}^{R} \beta_r S^*(J_r). \tag{3.18}$$

The remarkable thing about this result is that it holds for any cut W_l in addition to the minimal cuts and thus brings the bulk inequality in the set of holographic entropy inequalities. This requires the mapping f to be $\{0,1\}^L \to \{0,1\}^R$ with an appropriate initial condition, keeping the system within the correct boundary subsystems.

Moreover, they generalize the already known inequalities starting from the infinite, cyclic group of them:

$$\sum_{i=1}^{N} S((A_i \dots A_{i+l-1})(A_{i+l} \dots A_{i+l+k-1})) - S(A_{i+l} \dots A_{i+l+k-1}) \geq S(A_1 \dots A_N), \tag{3.19}$$

where the summation on the left hand side happens over the modulo of N in the so called conditional entropies. By considering the cases where both the monogamy of mutual information and the strong subadditivity are satisfied, namely setting $N = 2k + 1$ and $l = 1$, the resulting generalization of the cyclic inequalities is

$$\sum_{i=1}^{N} S(A_i | A_{i+1} \dots A_{i+k}) \geq S(A_1 \dots A_N), \tag{3.20}$$

where $S(A_i|A_{i+1} \dots A_{i+k})$ is the conditional entropy, defined as

$$S(A_i|A_{i+1}) = S(A_i, A_{i+1}) - S(A_{i+1}), \tag{3.21}$$

which corresponds to a finite number of inequalities. The reason using (3.20) is useful is that using only the strong subadditivity and monogamy of the mutual information is not enough for five or more regions. In that case, we have to consider additional inequalities that cannot be described with the two already familiar inequalities and thus (3.20) is one of these additional inequalities we must consider. For five regions, it becomes

$$S(A|BC) + S(B|CD) + S(C|DE) + S(D|EA) + S(E|AB) \geq S(ABCDE), \tag{3.22}$$

but it is important to note this is only one of the additional inequalities valid for five or more regions. However, together these three, the monogamy of the mutual information (1.15), strong subadditivity (3.2) and cyclic inequality for five regions (3.22), give the stabilizer inequalities for corresponding quantum system. This means that, the entropies must be stabilizing entropies. The term "stabilizing" refers to the stabilizer codes, which is a subclass of quantum error correction codes [43]. The other entropy inequalities presented by [8] for five regions are

1.

$$\begin{aligned} &2S(ABC) + S(ABD) + S(ABE) + S(ACD) + S(ADE) + S(BCE) \\ &\quad \geq S(AB) + S(ABCE) + S(ABDE) + S(AC) + S(AD) \\ &\quad + S(BC) + S(BE) + S(DE) \end{aligned} \tag{3.23}$$

2.

$$\begin{aligned} &S(ABE) + S(ABC) + S(ABD) + S(ACD) + S(ACE) + S(ADE) \\ &\quad + S(BCE) + S(BDE) + S(CDE) \geq +S(AB) + S(ABCE) + S(ABDE) \\ &\quad + S(AC) + S(ACDE) + S(AD) + S(BCD) + S(BE) + S(CE) + S(DE) \end{aligned} \tag{3.24}$$

3.

$$\begin{aligned} &S(ABC) + S(ABD) + S(ABE) + S(ACD) + S(BCE) + S(DE) \\ &\quad \geq S(AB) + S(ABCD) + S(ABCE) + S(AC) + S(ADE) \\ &\quad + S(B) + S(C) + S(D) + S(E) \end{aligned} \tag{3.25}$$

4.

$$\begin{aligned} &3S(ABC) + 3S(ABD) + 3S(ACE) + S(ABE) + S(ACD) + S(ADE) \\ &\quad + S(BCD) + S(BCE) + S(BDE) + S(CDE) \geq 2S(AB) + 2S(ABCD) \\ &\quad + 2S(ABCE) + 2S(AC) + 2S(BD) + 2S(CE) + S(ABDE) + S(ACDE) \\ &\quad + S(AD) + S(AE) + S(BC) + S(DE). \end{aligned} \tag{3.26}$$

These inequalities are independent from one another and can be associated with a certain facets of the five-region entropy cone. Still, these are only one family of the full, infinite set of inequalities possible to find for five regions. As a side note for the states lying on the boundary between holographic and non-holographic states, they are suggested to have entanglement entropy corresponding to the extreme rays of the entropy cone. Interesting addition is that in the framework of gravity, these extremal states are conjectured to correspond to wormhole geometries [34].

4 Evaluation of probes

When we start from higher temperature and begin to lower it, we can calculate the Wilson loops for the corresponding geometries and from the behavior of the Wilson loop we see whether the theory is deconfining or confining. In fact, next we will demonstrate how the lowering of the temperature moves the geometry from deconfining to the confining. In addition, for each geometry we shall visualize the entanglement wedge cross section E_W. From the reach of the Wilson loops compared to the reach of the wedge, we can see whether or not the Wilson loops are inside the wedge, and thus conclude if the subregion duality is satisfied.

The metric we wish to examine in the deconfining geometry is

$$g = \frac{R^2}{z^2}(-\frac{b(z)}{a(z)^2}dt^2 + \frac{a(z)^2}{b(z)}dz^2 + d\vec{x}^2), \tag{4.1}$$

in which R is the curvature radius of the spacetime. Now, we can choose the parametrization of $a(z) = 1$ which follows the Schwarzschild metric. In the Schwarzschild black hole metric, the radius of the spacetime can be marked with R and then scaled to $R = 1$. This leads us to the metric we refer to as the deconfining one:

$$g = \frac{R^2}{z^2}\left(-b(z)dt^2 + \frac{1}{b(z)}dz^2 + d\vec{x}^2\right). \tag{4.2}$$

This is dual to the quantum field theory at a finite temperature. In (4.2), the $b(z)$ is defined as $b(z) = 1 - \frac{z^4}{z_*^4}$, where z_h marks the black hole horizon coordinate. We can work with this metric in the units of temperature, which effectively means that $z_h = R = 1$. This is the notation we will use from now on.

Let us discuss about the confining background, which is the geometry where our bulk space has an ending at $z = z_0$. Considering the Poincaré patch, the z is the radial coordinate. This causes the mass gap, since the space ends to a non-zero value [16]. When we consider the strings hanging from the boundary, we can encounter only the configuration of connected string. This is because the disconnected strings would have no place to end, when we consider that they do not reach all the way to the end point, as visualized in the Figure 8. The possible "disconnected" configuration can be obtained if we consider the strings that have endpoints at the endpoint $z = z_0$. However, even in this case the strings can be thought to be connected at the endpoint. We can easily obtain the confining geometries from the black hole metric (4.2) by double Wick rotation. The confining geometry we are using is the same as in [28], namely

$$g = \frac{R^2}{z^2}(-dt^2 + \frac{dz^2}{b(z)} + d\vec{x}_{d-3}^2 + b(z)dx_{\text{circle}}^2), \tag{4.3}$$

where $b(z) = 1 - \frac{z^d}{z_h^d}$. We will consider the same $\mathcal{N} = 4$ Yang-Mills theory as before, but this time our space is $\mathbb{R}^3 \times S^1$. The metric for $d = 4$ is

$$g = \frac{R^2}{z^2}(-dt^2 + \frac{dz^2}{1 - \frac{z^d}{z_h^d}} + d\vec{x}^2 + (1 - \frac{z^d}{z_h^d})dx_{\text{circle}}^2) \tag{4.4}$$

$$= \frac{R^2}{z^2}(-dt^2 + \frac{dz^2}{1 - \frac{z^4}{z_h^4}} + d\vec{x}^2 + (1 - \frac{z^4}{z_h^4})dx_{\text{circle}}^2). \tag{4.5}$$

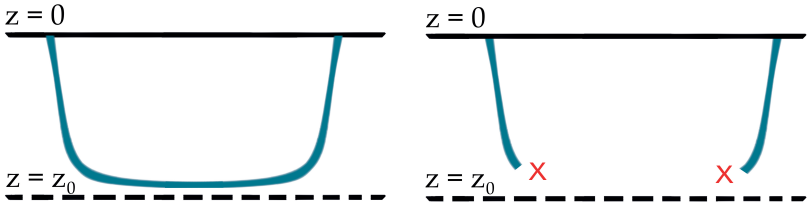

Figure 8: The string configuration for the confining geometry. On the left, we have the connected configuration. On the right, we have the non-possible disconnected configuration, where the strings have no endpoints.

Next, we will talk more about the reach of the probes and the bulk and evaluate the chosen probes in these two geometries.

4.1 Reach of the bulk and entanglement wedge

In this chapter, we will go through the probes introduced in earlier chapters. We shall evaluate the probes for both deconfining and confining geometries. These probes are the entanglement entropy, (spatial) Wilson loops, 't Hooft loops, entanglement wedge cross-section and two-point functions. This chapter will demonstrate on a fundamental level how the two chosen geometries vary from each other and how the behavior and reach of the embedding of these probes compare to the embedding and location of the entanglement wedge. In this context, we can use the term "reach" of the bulk and probes. The probes can be thought to have a certain reach, that essentially is the width $l(z_s)$. In the case of the subregion duality, the reach of the probes should always be less than the reach of the entanglement wedge.

In [6], they study the probes extended beyond the limit of the entanglement wedge with hope to understand how far does the Ryu-Takayanagi surface $m(B_{d-1})$ for the boundary subregion B_{d-1} reach. In detail, the bulk metric of considered AdS is reconstructed, which corresponds to possibilities of the reconstructed bulk metric reaching further than the entanglement wedge. They suggest that, either there is information about the bulk in the boundary subregion in addition to the entanglement wedge or that, for extremal 2-surfaces anchored in the given subregion, the subregion fails to have all the information about the areas of those surfaces. These suggestions challenge the current understanding of the subregion duality. In particular, we can evaluate probes such as Wilson lines and loops in such bulk metrics to find whether the reach of them is beyond the entanglement wedge as well or not. It has been stated ([35],[14]) that in the boundary CFT, the expectation values of these loops correspond to the particular areas of the extremal surfaces that lie in the boundary.

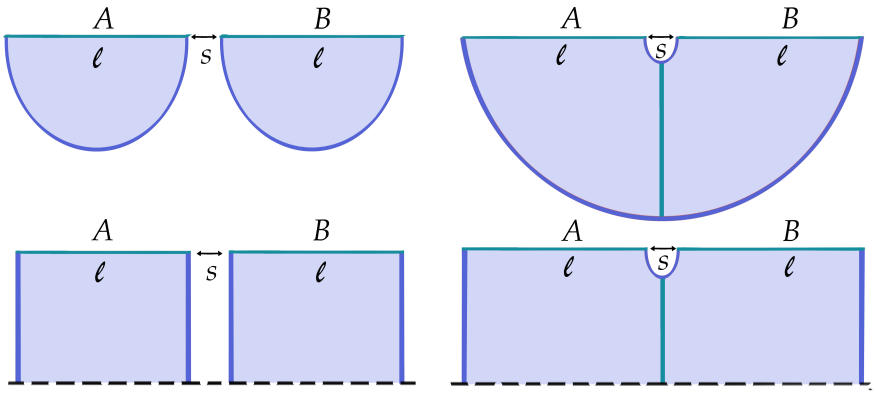

Figure 9: The schematics for the four different phases with two regions A and B, corresponding to two strips. The dashed black line is the horizon $z = z_h$. Notice that only two of these phases give nonzero entanglement wedge, which is the cyan vertical line on the right top and right bottom phases.

Now, we choose to study the case with different background geometry, such as those in [29] and [28]. In addition to the spatial Wilson loops, we can evaluate the 't Hooft loops and 2-point functions considering the same questions about the reach of these probes compared to the reach of the entanglement wedge. After evaluating these, it is then possible to map these probes to the entanglement wedge to see if they fall in or out of the wedge. Related to this, we can evaluate the entanglement entropy for both geometries. We have chosen two different bulk geometries to evaluate these probe, introduced as deconfining and confining geometries. Note that, when we mention the deconfining geometry, we refer to the geometry with the black hole. The method of obtaining either metric from the other one is in this case called the double Wick rotation.

4.2 Spatial Wilson loop

Deconfining bulk geometry

Spatial Wilson loops in asymptotically AdS_5 are presented as rectangles in (x_1, x_2)-plane, namely by considering a string that ends at the boundary of our AdS_5. This embedding gives us the induced metric as

$$\hat{g} = \frac{1}{z^2}\left(\left(\frac{1}{b(z) + x'(z)^2}\right)dz + d\vec{x}_{d-2}^2\right). \tag{4.6}$$

From here, we obtain the Lagrangian density:

$$\mathcal{L} = \frac{1}{z^2}\sqrt{g_{zz}(z) + x'(z)^2}, \tag{4.7}$$

and now we can use the Euler-Lagrange equations of motions to solve for the conserved quantity, namely solving the equation

$$\partial_{x'(z)}\mathcal{L} = \frac{1}{z_*^2} \tag{4.8}$$

for $x'(z)$, which yelds

$$x'(z) = \frac{z^2}{\sqrt{-z^4 + z^8 + z_*^4 - z^4 z_*^4}}. \tag{4.9}$$

Therefore, the strip width integral in terms of this conserved quantity is

$$l(z_*) = 2\int_0^{z_*} x'(z)dz = 2\int_0^{z_*} \frac{z^2}{\sqrt{-z^4 + z^8 + z_*^4 - z^4 z_*^4}} dz. \tag{4.10}$$

For the Wilson loop, we need to evaluate the action in (2.58). Plugging our Lagrangian density with the conserved quantity (4.9) into the Nambu-Goto action (2.66), we have

$$S_{NG} = \frac{TR^2}{\pi\alpha'} \int_\epsilon^{z_*} \frac{z_*^2}{z^2} \sqrt{\frac{g_{zz}(z)}{1 - \frac{z^4}{z_*^4}}} dz, \tag{4.11}$$

where $g_{zz}(z) = \frac{1}{1-z^4}$, and the divergence is omitted by introducing ϵ as a cutoff. Now, the main interest in the loop probes is fundamentally the potential between quarks and namely, what is the effect of the potential compared to the case where quarks would be free. For this reason, from the action for two quarks, we need to subtract the action of two free quarks, as introduced in (2.61). In the case of deconfining geometry, we in fact have few different possibilities for the subtracted term. We choose to subtract the part where the string reaches from the horizon to the boundary [10].

Now, from the equations of motions we see that the disjoint configuration is allowed. This is because the area of the piece along the horizon is non-vanishing. We should then continue with area regularization, to get rid of the divergence in the action. This results in

$$S_{NG}^{reg} = \frac{TR^2}{\pi\alpha'}\frac{1}{\epsilon} - \frac{TR^2}{\pi\alpha'}\frac{1}{z_*} - \frac{TR^2}{\pi\alpha'}\int_0^{z_*} \frac{1}{z^2}\left(\sqrt{\frac{g_{zz}(z)}{1 - \frac{z^4}{z_*^4}}} - 1\right) dz, \tag{4.12}$$

where we used an UV-cutoff to get rid of the divergence and regularize it by taking the divergence term with ϵ out. We shall call the regularized version S_{NG}^{reg}. This leads to the expectation value of the spatial Wilson loops:

$$\langle W(\partial B)\rangle = e^{-S_{NG}} \tag{4.13}$$

$$= \exp\left(-\frac{TR^2}{\pi\alpha'}\frac{1}{\epsilon} + \frac{TR^2}{\pi\alpha'}\frac{1}{z_*} + \frac{TR^2}{\pi\alpha'}\int_0^{z_*} \frac{1}{z^2}\left(\sqrt{\frac{g_{zz}(z)}{1 - \frac{z^4}{z_*^4}}} - 1\right) dz\right). \tag{4.14}$$

This regularized version of Wilson loop, corresponding to the quark-antiquark potential is shown in Figure 10 as the function of l (4.10) together with the potential in confining geometry. In that figure, we see a phase transition between two phases. The dominant phase is the one where the string has broken and for which the potential is identically zero, since we have used this phase as a regulator.

Confining geometry

We will now introduce the embedding with $t = \text{const.}$ and $x = \text{const.}$. The induced metric on this surface is then

$$\hat{g} = \frac{1}{z^2}\left(\frac{dz^2}{b(z)} + b(z)dx^2_{\text{circle}}\right), \tag{4.15}$$

where $b(z) = 1 - z^4$, and we have used again the units in which $R = z_h = 1$. We can then get the equations of motion and solve that for the conserved quantity x'^2_{circle}, yielding

$$x'^2_{\text{circle}} = \frac{z^2}{\sqrt{1-z_*^4}\sqrt{z_*^4(1-z^4) - z^4(1-z_*^4)}}, \tag{4.16}$$

where z_* is the turning point. This gives the $l(z_*)$ integral as

$$l(z_*) = 2\int_0^{z_*} \frac{z^2}{\sqrt{1-z_*^4}\sqrt{z_*^4(1-z^4) - z^4(1-z_*^4)}}dz. \tag{4.17}$$

The Nambu-Goto action (2.66) with $R = z_h = 1$ is then

$$S_{NG} = \frac{T}{\pi\alpha'}\int_0^{z_*} \frac{1}{z^2}\sqrt{\frac{1}{b(z)} + b(z)x'_{\text{circle}}(z)^2}dz. \tag{4.18}$$

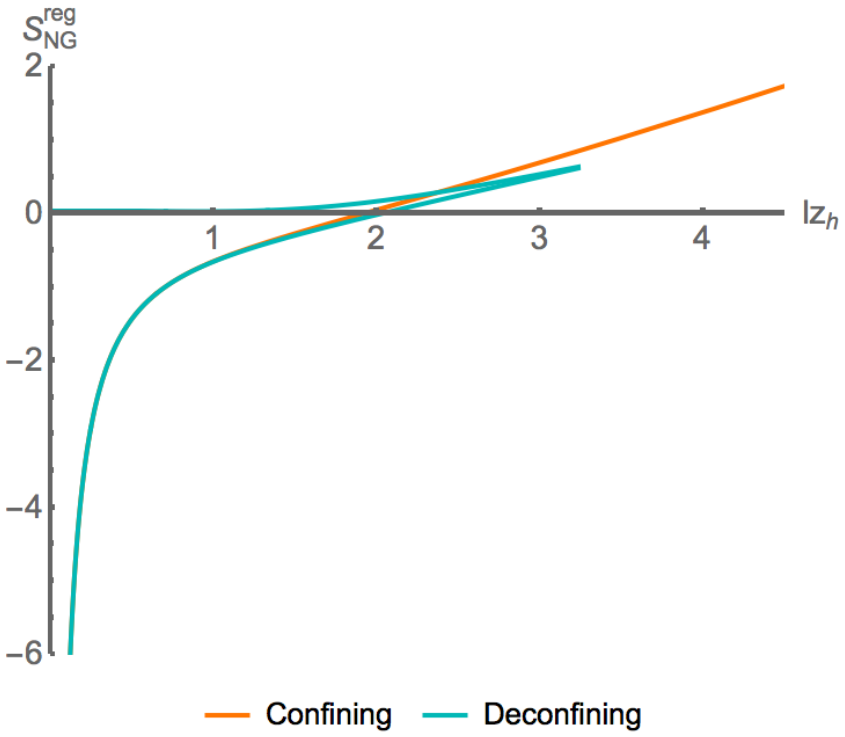

Figure 10: Regularized actions for both geometries as a function of l.

We now need to subtract from the action the part where the string reaches the bottom of our geometry. This gives us the regularized version of the action:

$$S_{NG}^{\text{reg}} = \frac{T}{\pi\alpha'}\int_0^{z_*}\left(\frac{1}{z^2}\sqrt{\frac{1}{1-z^4}} + \frac{1}{1-z_*^4}\frac{z^4}{z_*^4(1-z^4)-z^4(1-z_*^4)} - \frac{1}{z^2}\right)dz - \frac{T}{\pi\alpha'}\frac{1}{z_*} + \frac{T}{\pi\alpha'}\frac{1}{\epsilon}. \tag{4.19}$$

We will use the regularized action to evaluate the Wilson loop

$$\langle W\rangle = e^{-S_{NG}}. \tag{4.20}$$

Essentially, the quark-antiquark potential is the logarithm of the Wilson loop, where the action was regularized. This is visualized in the Figure 13 as a function of $l(z_*)$, where we can see the difference of the behavior of this probe in deconfining and confining geometries.

4.3 't Hooft loop

Deconfining geometry

Since we work with bulk geometries that have constant dilaton, we can expect the 't Hooft loop, introduced in (2.67), to behave similarly to the Wilson loop. We obtain

$$H(\partial B) = e^{-S_{D1}}, \tag{4.21}$$

where S_{D1} is the action for the D1-brane involving the term for dilaton. Thus, we have

$$H(\partial B) = \frac{\tilde{T}R^2}{\pi\alpha'}\int_\epsilon^{z_*} e^{-\phi}\frac{z_*^2}{z^2}\sqrt{\frac{g_{zz}(z)}{z_*^4-z^4}}dz. \tag{4.22}$$

Now, since this deconfining geometry does not involve non-constant dilaton, namely the scalar field is constant, the term in our action corresponding to the dilaton acts only as constant coefficient. This results in shifted version of the Wilson loop, where the shift depends on the value of the dilaton. If we have $e^{-\phi} = 1$, the result yelds no shift.

Confining geometry

Once again, we are using the definition of (holographic) 't Hooft loop (2.67) which is

$$H(\partial B) = e^{-S_{D1}}, \tag{4.23}$$

As discussed with the previous geometry, only the non-constant dilaton fields alter to the behavior of the 't Hooft loop making it differ from the Wilson loop. Indeed, for this confining geometry, we have the dilaton to be constant, and therefore the behavior of the 't Hooft loop is the same that of the Wilson loop. The difference comes from a constant dilaton term: we have additional coefficient to the loop, making 't Hooft loop again the shifted version of the Wilson loop for the confining geometry. If we choose to use the notation $e^{-\phi} = 1$, the result is yields no shift.

4.4 Entanglement wedge cross section

Deconfining geometry

Furthermore, our goal is to extremize the world sheet of a string hanging between quark and anti-quark. Using the same embedding as with the Wilson loops, our strip width integral is

$$l(z_*) = 2\int_0^{z_*} x'(z)dz = 2\int_0^{z_*} \frac{z^2}{-z^4+z^8+z_*^4-z^4z_*^4}dz. \tag{4.24}$$

Interestingly, this can be written as series using the Pochhammer symbol $(a)_m$ as [17]

$$l(z_*) = 2\sqrt{\pi}z_* \sum_{m=0}^{\infty} \frac{1}{m!(1+md)} \left(\frac{1}{2}\right)_m \frac{\Gamma\left(\frac{d(m+1)}{2(d-1)}\right)}{\Gamma\left(\frac{1+md}{2(d+1)}\right)} \left(\frac{z}{z_*}\right)^{md}, \tag{4.25}$$

which in our case is

$$l(z_*) = 2\sqrt{\pi}z_* \sum_{m=0}^{\infty} \frac{1}{m!(1+4m)} \left(\frac{1}{2}\right)_m \frac{\Gamma\left(\frac{2(m+1)}{3}\right)}{\Gamma\left(\frac{1+4m}{6}\right)} \left(\frac{z}{z_*}\right)^{4m}. \tag{4.26}$$

This can be written as series using the Pochhammer symbol $(a)_m$ as [17]

$$l(z_*) = 2\sqrt{\pi}z_* \sum_{m=0}^{\infty} \frac{1}{m!(1+md)} \left(\frac{1}{2}\right)_m \frac{\Gamma\left(\frac{d(m+1)}{2(d-1)}\right)}{\Gamma\left(\frac{1+md}{2(d+1)}\right)} \left(\frac{z}{z_*}\right)^{md}, \tag{4.27}$$

which in our case is then

$$l(z_*) = 2\sqrt{\pi}z_* \sum_{m=0}^{\infty} \frac{1}{m!(1+4m)} \left(\frac{1}{2}\right)_m \frac{\Gamma\left(\frac{2(m+1)}{3}\right)}{\Gamma\left(\frac{1+4m}{6}\right)} \left(\frac{z}{z_*}\right)^{4m}. \tag{4.28}$$

To evaluate the entanglement wedge cross section, we either perform the integral analytically as in [28], or evaluate it numerically. For the analytical approach, the entanglement wedge cross section is proportional to the area of the hypersurface, assuming symmetric configuration, such as presented in the Figure 9, where the widths of the two strips are equal. The separation of the two strips is marked with s. Let the hypersurface be called Γ, in which case the entanglement wedge cross section (with $z_h = R = 1$) follows as

$$E_W = \frac{1}{4G_N^{(d+1)}} \int vol\,(\Gamma) \tag{4.29}$$

$$= \frac{VR^3}{8G_N^{(5)}z_h^2} \left(\left(\frac{z}{z_h}\right)^{-2} {}_2F_1\left(\frac{1}{2}, \frac{-1}{2}, \frac{1}{2}, \frac{z^4}{z_h^4}\right) \right)_{z_*(2l+s)}^{z_*(s)} \tag{4.30}$$

$$= \frac{V}{8G_N^{(5)}} \left((z)^{-2} {}_2F_1\left(\frac{1}{2}, \frac{-1}{2}, \frac{1}{2}, z^4\right) \right)_{z_*(2l+s)}^{z_*(s)} \tag{4.31}$$

The limits of this integration can be realized from the Figure 9. The lower limit is the z_* evaluated at the total width of strips plus the separation, namely at $2l + s$. The higher limit is z_* at only the separation width, which is marked with s. For the numerical approach, we can first use the iterated values of $l(z_*)$ and its reverse, $z_*(l)$ to get the entanglement entropy. The entanglement wedge cross section is then integral in the region that satisfies $2S(l) > S(2l + s) + S(s)$, where S is the entanglement entropy:

$$E_W = \int_{z_*(s)}^{z_*(2l+s)} \frac{1}{z^3}\sqrt{\frac{1}{1-z^4}}dz. \tag{4.32}$$

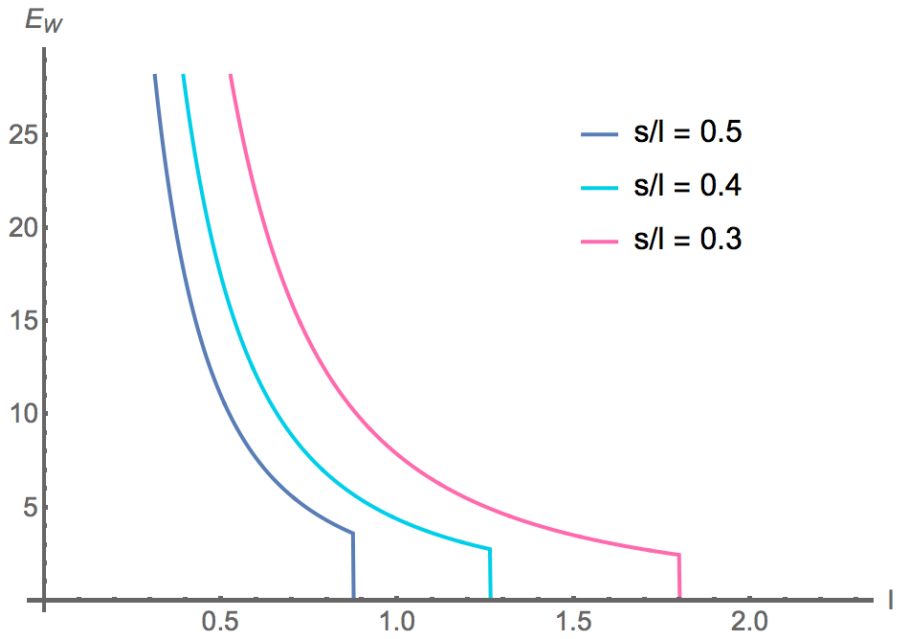

Figure 11: Entanglement wedge cross section for three different values of s/l.

Since the ratio of s/l needs to be fixed for visualization of the E_W, we have chosen three different values of the s/l ratio shown in Figure 11. In this figure, we see the phase transition happening at certain l, which corresponds to the transition of connected entanglement wedge to non-connected one, resulting in vanishing cross section.

Confining geometry

To evaluate the entanglement wedge cross section for the confining geometry, we will use similar embedding as with the Wilson loop calculation. We have the strip width integral as

$$l(z_*) = 2\int_0^{z_*} \frac{z^2}{\sqrt{1-z_*^4}\sqrt{z_*^4(1-z^4)-z^4(1-z_*^4)}}dz. \tag{4.33}$$

Furthermore, we note that the turning point z_* is not to be explicitly evaluated but used with numerical approximation for the further evaluation of E_W. The entanglement wedge cross section follows as

$$E_W = \int_{z_*(s)}^{z_*(2l+s)} \frac{1}{z^3} \frac{1}{\sqrt{1-z^4}} dz. \tag{4.34}$$

For the confining geometry, we have again four possible phases for the entanglement wedge. These configurations are realized in the Figure 9. The entanglement wedge cross section for confining geometry is visualized in the Figure 12 for three different values of s/l. We notice, that this time we have two phase transitions. The first one happens when we encounter the critical value where $2l + s = l^{(4)}_{crit}$ and the second transition is when $s = l^{(4)}_{crit}$. Here the $l^{(4)}_{crit}$ can be derived as in [28].

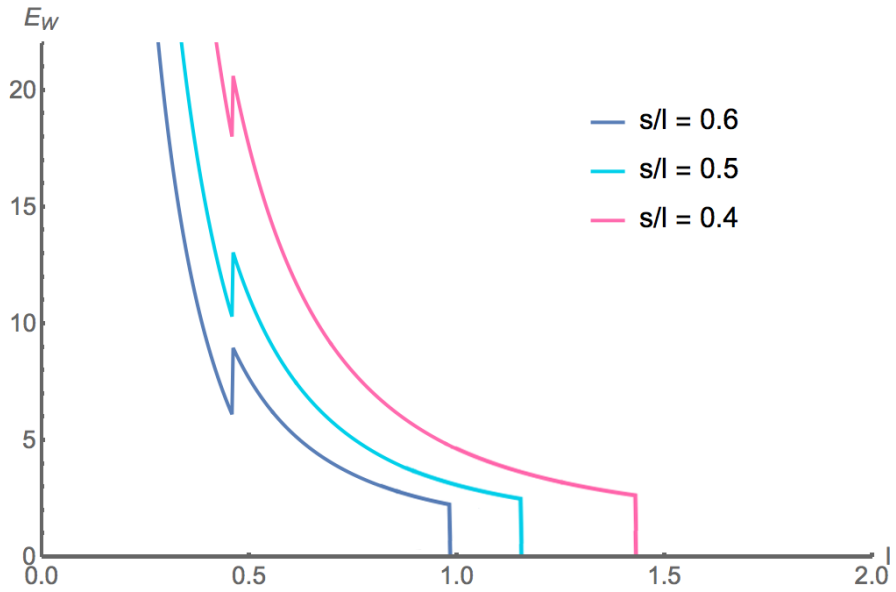

Figure 12: Entanglement wedge cross section for three different values of s/l.

4.5 Two-point function

Deconfining geometry

We will then study the massive particle geodesics to obtain the two-point function of heavy operators. Using the embedding in (t, x_1) plane, we can again use the Euler-Lagrange equations of motion to find the conserved quantity $x'(z)$ as

$$x'(z) = \frac{z}{z_*} \frac{g_{zz}(z)}{1 - \left(\frac{z}{z_*}\right)^2} dz, \tag{4.35}$$

where $g_{zz}(z) = \frac{1}{1-z^4}$. We use this conserved quantity to find the $l(z_*)$:

$$l(z_*) = 2\int_0^{z_*} \frac{z}{z_*} \frac{\sqrt{g_{zz}(z)}}{\sqrt{1-\left(\frac{z}{z_*}\right)^2}} dz. \tag{4.36}$$

Now, we have everything we need to evaluate the functionality A needed for the two-point function. Plugging in the $l(z_*)$ yields

$$A = 2R\int_\epsilon^{z_*} \frac{1}{z} \frac{\sqrt{g_{zz}(z)}}{\sqrt{1-\left(\frac{z}{z_*}\right)^2}} dz \tag{4.37}$$

$$= 2\int_\epsilon^{z_*} \frac{1}{z} \frac{\sqrt{g_{zz}(z)}}{\sqrt{1-\left(\frac{z}{z_*}\right)^2}} dz \tag{4.38}$$

$$= 2\ln\left(\frac{1}{\epsilon}\right) - 2\ln\left(\frac{1}{z_*}\right) + 2\int_0^{z_*} \frac{1}{z}\left(\frac{\sqrt{g_{zz}(z)}}{\sqrt{1-\left(\frac{z}{z_*}\right)^2}} - 1\right) dz. \tag{4.39}$$

where on the second line we have implemented the $z_h = R = 1$, so that the metric component g_{zz} reduces to

$$g_{zz}(z, z_h = 1) = \frac{1}{1-z^4}. \tag{4.40}$$

In the last line of (4.37), we have omitted the divergent term away from the integral, leaving us with finite integral from 0 to z_*. Using this, the two-point function becomes

$$\langle \mathcal{O}(t,\vec{x})\mathcal{O}(t,\vec{y})\rangle = \lim_{\epsilon\to 0} \epsilon^{-2\Delta} e^{-\Delta A}, \tag{4.41}$$

where Δ is the dimension of the operator. By plugging in the A, (4.41) takes the form

$$\langle \mathcal{O}(t,\vec{x})\mathcal{O}(t,\vec{y})\rangle = \lim_{\epsilon\to 0} \epsilon^{-2\Delta} \exp\left(\Delta\ln(\frac{1}{\epsilon}) - \ln(\frac{1}{z_*})\right) \cdot \exp\left(\int_0^{z_*} \frac{1}{z}\left(\frac{1}{\sqrt{1-z^4}\sqrt{1-\frac{z^2}{z_*^2}}} - 1\right) dz\right).$$

This is shown in the Figure 13 as $\log_{10}(\langle \mathcal{O}(t,\vec{x})\mathcal{O}(t,\vec{y})\rangle)$ with $\Delta = 1$ and the term with ϵ omitted.

Confining geometry

For the confining geometry, we shall again look the geodesics of a massive particle to get the two-point function. We have the induced metric with $R = z_h = 1$ as

$$\hat{g} = \frac{1}{z^2}\left(-dt^2 + \left(\frac{1}{b(z)} + b(z)x'^2_{\text{circle}}\right) dz\right) \tag{4.42}$$

which means we will solve the equations of motion with Lagrangian density

$$\mathcal{L} = \frac{1}{z^2}\sqrt{-\left(\frac{1}{1-z^4} + (1-z^4)x'^2_{\text{circle}}\right)} \tag{4.43}$$

to obtain the conserved quantity as

$$x'^2_{\text{circle}} = \frac{z^2}{(1-z^4)\sqrt{z_*^4 - z^4(z_*^4-1)}}. \tag{4.44}$$

We will plug this into the integrals for $l(z_*)$ and $A(z_*)$:

$$l(z_*) = 2\int_0^{z_*} \frac{z^2}{(1-z^4)\sqrt{z_*^4 - z^4(z_*^4-1)}}dz \tag{4.45}$$

$$A(z_*) = 2\int_0^{z_*} \frac{z_*}{(z^4-1)\sqrt{z_*^4 - z^4(z_*^4-1)}}dz - 2\ln\left(\frac{1}{z_*}\right). \tag{4.46}$$

Now we have everything we need for the two-point function. Similarly to the deconfining geometry, we shall use the formulation

$$\langle \mathcal{O}(t,\vec{x})\mathcal{O}(t,\vec{y})\rangle = \lim_{\epsilon\to 0} \epsilon^{-2\Delta} e^{-\Delta A}, \tag{4.47}$$

which for our $A(z_*)$ is shown in Figure 13 together with the two-point function of the deconfining geometry.

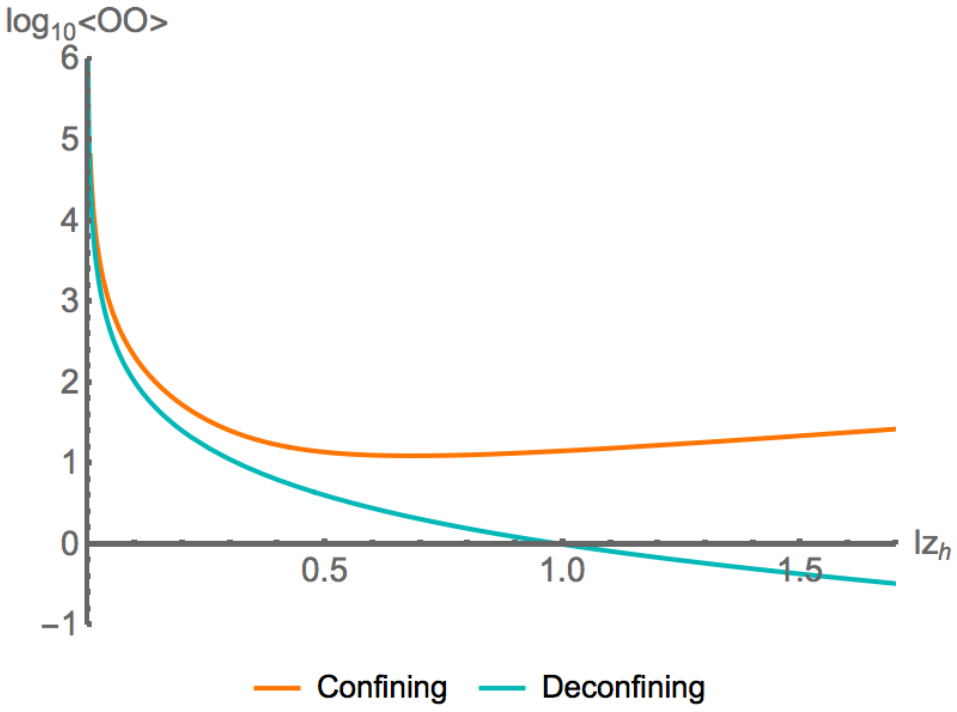

Figure 13: 2-point function on the logarithm scale for both geometries. Note that while $z_h = 1$, its units are still on the horizontal axis with the width l. For the small values of l, we see how the correlation is highly similar in both geometries and differs when the value of l is increased.

4.6 Entanglement entropy

Deconfining geometry

The first probe we will evaluate for this geometry is the (holographic) entanglement entropy. We shall find the Ryu-Takayanagi surface, for which we can find the entropy according to the proposal (2.22). The embedding we use is motivated as follows: The bulk surface can be thought as spanning the x_2 and x_3 directions. This leaves us with embedding in $z \mapsto x_1(z)$. Therefore, we can solve the conserved quantity $x_1'(z)$ from the equations of motion, obtaining

$$x_1'(z) = \left(\frac{z}{z_*}\right)^3 \frac{1}{\sqrt{1-z^4}} \frac{dz}{\sqrt{1-\left(\frac{z}{z_*}\right)^6}}, \tag{4.48}$$

where z_* is the bulk turning point. The strip width integral can be written in terms of this, namely

$$l(z_*) = 2\int_0^{z_*} x_1'(z)dz = 2\int \left(\frac{z}{z_*}\right)^3 \frac{1}{\sqrt{1-z^4}} \frac{dz}{\sqrt{1-\left(\frac{z}{z_*}\right)^6}}. \tag{4.49}$$

The entanglement entropy is thus

$$S_A(z) = 2\int_\epsilon^{z_*} \frac{1}{z^3} \frac{1}{\sqrt{1-z^4}} \frac{dz}{\sqrt{1-\left(\frac{z}{z_*}\right)^6}} \tag{4.50}$$

$$= 2\int_0^{z_*} \frac{1}{z^3} \left(\frac{1}{\sqrt{1-z^4}\sqrt{1-\left(\frac{z}{z_*}\right)^6}} - 1 \right) dz - \frac{2}{z_*^2}, \tag{4.51}$$

where in the last row we have omitted the epsilon term from the integral, and focus on the terms contributing to the behavior of the entropy. This is visualized as a function of l in the Figure 14 together with the entanglement entropy in the confining geometry.

The entanglement entropies in different phases are

$$S(A) = 2S(l) \tag{4.52}$$

$$S(B) = S(2l+s) \tag{4.53}$$

$$S(AB) = S(s). \tag{4.54}$$

Confining geometry

The entanglement entropy as a function of the turning point is obtained from the RT-formula 2.22. For that, we use an embedding with constant t and $dx = 0$. This gives the induced metric as

$$\hat{g} = \frac{1}{z^2}\left(\frac{dz^2}{b(z)} + d\vec{x}_1^2 + b(z)dx_{\text{circle}}^2\right). \tag{4.55}$$

Solving the equations motion for the conserved quantity gives us the $l(z_*)$ integral as

$$l(z_*) = 2\int_0^{z_*} \left(\frac{z}{z_*}\right)^3 \frac{dz}{(1-z^4)\sqrt{1-\left(\frac{z}{z_*}\right)^6 \frac{1-z_*^4}{1-z_*4}}}. \tag{4.56}$$

The entanglement entropy is a function of $l(z_*)$, since the we can obtain the RT-surface using the strip width integral. The entanglement entropy is

$$S_A = 2\int_0^{z_*} \left(\frac{1}{z^3}\frac{1}{\sqrt{1-\left(\frac{z}{z_*}\right)^6 \frac{1-z_*^4}{1-z^4}}}\right) dz - \frac{2}{z_*^2}, \tag{4.57}$$

where we have omitted any constant coefficient and subtracted the divergent part away from the integral.

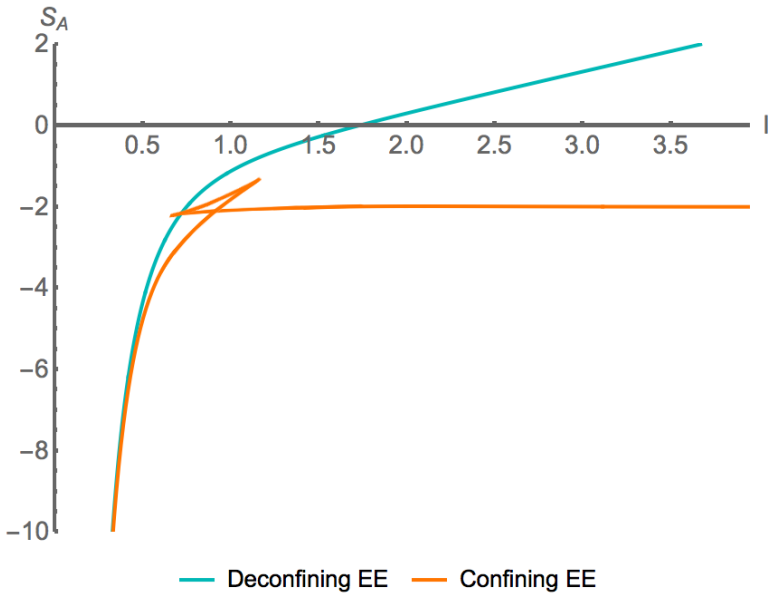

Figure 14: Entanglement entropy for the confining geometry together with the entanglement entropy for the deconfining geometry as a function of l.

The behavior of this entanglement entropy is shown in Figure 14 as a function of l, compared to the entanglement entropy of the deconfining geometry. As we see, with confining geometry we have a phase transition. As mentioned, the entanglement entropy of deconfining geometry is linear with large values of $l(z_*)$ all the way to the horizon. With the confining geometry, this is not the case. Instead, when we approach the horizon, we have a phase transition into the phase of $\mathcal{O}(N^0)$.

5 Discussion and conclusion

We introduced holography as a tool for addressing the question of entanglement. Using the dual properties of the considered geometries, we can evaluate the probes

introduced in the first sections. These probes are dependent on the bulk metric of the geometry. In the discussion of the entanglement entropy, we introduced not only the most fundamental inequalities, but the results on holographic entropy cone. These gave us guideline on what to expect and what to check when calculating the entanglement entropies for different geometries.

After evaluating the entanglement entropies for the deconfining AdS black brane background and the confining background, we could test not only the most fundamental entropy inequalities but the ones presented together with the holographic entropy cone for two regions, A and B.

Another research result addressed in this thesis was the bulk reconstruction while concentrating on its reach compared to the reach of the entanglement wedge. As discovered in [6], the bulk reconstruction can reach further than the entanglement wedge. Thus, evaluating the holographic probes for two different background geometries gives us insight about the localization of the probes themselves with respect to the bulk and entanglement wedge. As described earlier, the reach of these variables and the bulk reconstruction beyond the entanglement wedge would associate with violation of the subregion duality as we currently know it. In fact, such situation would point to reduced CFT living on the boundary of the entanglement wedge. The evaluations of the chosen probes was done in 4 dimension in this thesis. The result obeyed the subregion duality, namely the spatial Wilson loops for both deconfining and confining geometries lay inside the entanglement wedge. This is realized in Figure 15 with comparing the reach of the entanglement entropy to the reach of the potentials given by Wilson loop, as a function of l.

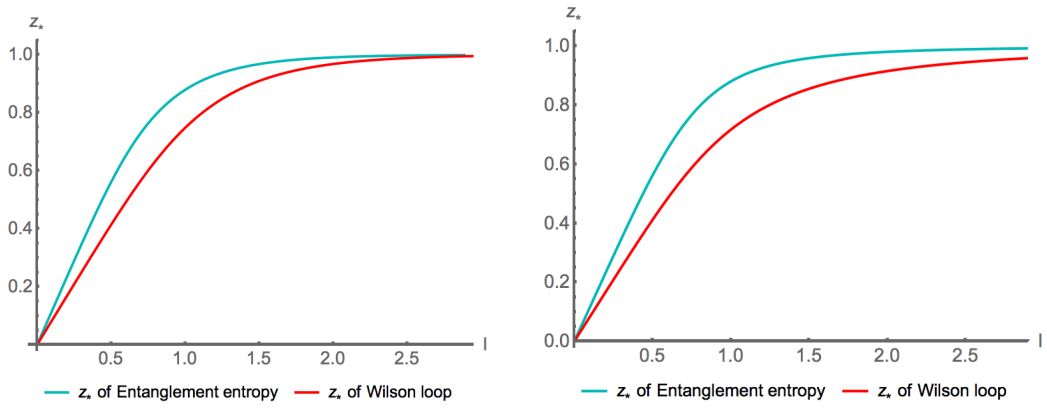

Figure 15: Left: the deconfining geometry. **Right:** the confining geometry. These figures present the embedding of the entanglement entropy compared to the embedding of the Wilson loop for both geometries. This means, we plot the z_* against the $l(z_*)$.

Even though the two geometries we worked with in this thesis did give us results that obey the subregion duality, this may not be true for arbitrary background geometries. There is second option for the probes to end outside the boundary of the entanglement wedge, and for non-trivial geometries we can not assume either one, and in fact the subregion duality in some of the non-trivial backgrounds may be

violated. The calculations of probes with respect to the reach of the entanglement wedge in such non-trivial geometries therefore are the target of future research.

References

[1] Cesar A. Agón, Elena Cáceres, and Juan F. Pedraza. Bit threads, Einstein's equations and bulk locality. 7 2020.

[2] Ofer Aharony, Steven S. Gubser, Juan Martin Maldacena, Hirosi Ooguri, and Yaron Oz. Large N field theories, string theory and gravity. *Phys. Rept.*, 323:183–386, 2000.

[3] Enrique Alvarez, Jorge Conde, and Lorenzo Hernandez. Codimension two holography. *Nucl. Phys. B*, 663:365–376, 2003.

[4] Shrobona Bagchi and Arun Kumar Pati. Monogamy, polygamy, and other properties of entanglement of purification. *Physical Review A*, 91(4):042323, 2015.

[5] Ning Bao, ChunJun Cao, Michael Walter, and Zitao Wang. Holographic entropy inequalities and gapped phases of matter. *JHEP*, 09:203, 2015.

[6] Ning Bao, Aidan Chatwin-Davies, Benjamin E. Niehoff, and Mykhaylo Usatyuk. Bulk Reconstruction Beyond the Entanglement Wedge. *Phys. Rev. D*, 101(6):066011, 2020.

[7] Ning Bao and Illan F. Halpern. Holographic Inequalities and Entanglement of Purification. *JHEP*, 03:006, 2018.

[8] Ning Bao, Sepehr Nezami, Hirosi Ooguri, Bogdan Stoica, James Sully, and Michael Walter. The Holographic Entropy Cone. *JHEP*, 09:130, 2015.

[9] Alexandre Belin, Nathan Benjamin, Alejandra Castro, Sarah M. Harrison, and Christoph A. Keller. $\mathcal{N} = 2$ Minimal Models: A Holographic Needle in a Symmetric Orbifold Haystack. *SciPost Phys.*, 8(6):084, 2020.

[10] Omer Ben-Ami, Dean Carmi, and Jacob Sonnenschein. Holographic Entanglement Entropy of Multiple Strips. *JHEP*, 11:144, 2014.

[11] Shawn X. Cui, Patrick Hayden, Temple He, Matthew Headrick, Bogdan Stoica, and Michael Walter. Bit Threads and Holographic Monogamy. *Commun. Math. Phys.*, 376(1):609–648, 2019.

[12] Jan de Boer. The Holographic renormalization group. *Fortsch. Phys.*, 49:339–358, 2001.

[13] R. Dougherty, C. Freiling, and K. Zeger. Networks, matroids, and non-shannon information inequalities. *IEEE Trans. Inf. Theor.*, 53(6):1949–1969, June 2007.

[14] Nadav Drukker, David J. Gross, and Hirosi Ooguri. Wilson loops and minimal surfaces. *Phys. Rev. D*, 60:125006, 1999.

[15] Souvik Dutta and Thomas Faulkner. A canonical purification for the entanglement wedge cross-section. 5 2019.

[16] Antón F. Faedo, David Mateos, David Pravos, and Javier G. Subils. Mass Gap without Confinement. *JHEP*, 06:153, 2017.

[17] Willy Fischler and Sandipan Kundu. Strongly Coupled Gauge Theories: High and Low Temperature Behavior of Non-local Observables. *JHEP*, 05:098, 2013.

[18] Michael Freedman and Matthew Headrick. Bit threads and holographic entanglement. *Commun. Math. Phys.*, 352(1):407–438, 2017.

[19] Jaume Gomis, Takuya Okuda, and Diego Trancanelli. Quantum 't Hooft operators and S-duality in N=4 super Yang-Mills. *Adv. Theor. Math. Phys.*, 13(6):1941–1981, 2009.

[20] Alex Hamilton, Daniel N. Kabat, Gilad Lifschytz, and David A. Lowe. Local bulk operators in AdS/CFT: A Boundary view of horizons and locality. *Phys. Rev. D*, 73:086003, 2006.

[21] Daniel Harlow. Jerusalem Lectures on Black Holes and Quantum Information. *Rev. Mod. Phys.*, 88:015002, 2016.

[22] Daniel Harlow and Hirosi Ooguri. Symmetries in quantum field theory and quantum gravity. 10 2018.

[23] Jonathan Harper and Matthew Headrick. Bit threads and holographic entanglement of purification. *JHEP*, 08:101, 2019.

[24] Patrick Hayden, Matthew Headrick, and Alexander Maloney. Holographic Mutual Information is Monogamous. *Phys. Rev. D*, 87(4):046003, 2013.

[25] Matthew Headrick and Veronika E. Hubeny. Riemannian and Lorentzian flow-cut theorems. *Class. Quant. Grav.*, 35(10):10, 2018.

[26] Matthew Headrick and Tadashi Takayanagi. A Holographic proof of the strong subadditivity of entanglement entropy. *Phys. Rev. D*, 76:106013, 2007.

[27] Veronika E. Hubeny. Extremal surfaces as bulk probes in AdS/CFT. *JHEP*, 07:093, 2012.

[28] Niko Jokela and Arttu Pönni. Notes on entanglement wedge cross sections. *JHEP*, 07:087, 2019.

[29] Niko Jokela and Arttu Pönni. Towards precision holography. 6 2020.

[30] Matti Järvinen. Quark-Antiquark Bound States in 1+1 Dimensional QCD. Master's thesis, U. Helsinki, 2004.

[31] Jonah Kudler-Flam and Shinsei Ryu. Entanglement negativity and minimal entanglement wedge cross sections in holographic theories. *Phys. Rev. D*, 99(10):106014, 2019.

[32] Biagio Lucini and Marco Panero. SU(N) gauge theories at large N. *Phys. Rept.*, 526:93–163, 2013.

[33] Yuri Makeenko. A Brief Introduction to Wilson Loops and Large N. *Phys. Atom. Nucl.*, 73:878–894, 2010.

[34] Juan Maldacena and Leonard Susskind. Cool horizons for entangled black holes. *Fortsch. Phys.*, 61:781–811, 2013.

[35] Juan Martin Maldacena. Wilson loops in large N field theories. *Phys. Rev. Lett.*, 80:4859–4862, 1998.

[36] Juan Martin Maldacena. The Large N limit of superconformal field theories and supergravity. *Int. J. Theor. Phys.*, 38:1113–1133, 1999.

[37] Horatiu Nastase. Introduction to AdS-CFT. 12 2007.

[38] Makoto Natsuume. *AdS/CFT Duality User Guide*, volume 903. 2015.

[39] Andrea Pelissetto and Ettore Vicari. Critical phenomena and renormalization group theory. *Phys. Rept.*, 368:549–727, 2002.

[40] Fabrizio Pucci. More on 't Hooft loops in N=4 SYM. *JHEP*, 11:161, 2012.

[41] Arttu Pönni. *Holographic Studies of Entanglement Measures*. PhD thesis, U. Helsinki, 2019.

[42] Alfonso V. Ramallo. Introduction to the AdS/CFT correspondence. *Springer Proc. Phys.*, 161:411–474, 2015.

[43] Joschka Roffe. Quantum error correction: an introductory guide. *Contemporary Physics*, 60(3):226–245, Jul 2019.

[44] Shinsei Ryu and Tadashi Takayanagi. Holographic derivation of entanglement entropy from AdS/CFT. *Phys. Rev. Lett.*, 96:181602, 2006.

[45] Richard J. Szabo. Quantum field theory on noncommutative spaces. *Phys. Rept.*, 378:207–299, 2003.

[46] Tadashi Takayanagi and Koji Umemoto. Entanglement of purification through holographic duality. *Nature Phys.*, 14(6):573–577, 2018.

[47] Kotaro Tamaoka. Entanglement Wedge Cross Section from the Dual Density Matrix. *Phys. Rev. Lett.*, 122(14):141601, 2019.

[48] Leung Terhal, Horodecki and DiVincenzo. The entanglement of purification. *Journal of Mathematical Physics*, 43(9):4286–4298, 2002.

[49] David Tong. String Theory. 1 2009.

[50] C. Tsallis. Possible generalization of boltzmann-gibbs statistics. *J. Statist. Phys.*, 52:479, 1988.

[51] Mark Van Raamsdonk. Lectures on Gravity and Entanglement. In *Theoretical Advanced Study Institute in Elementary Particle Physics: New Frontiers in Fields and Strings*, pages 297–351, 2017.

[52] Aron C. Wall. Maximin Surfaces, and the Strong Subadditivity of the Covariant Holographic Entanglement Entropy. *Class. Quant. Grav.*, 31(22):225007, 2014.